PLOS Computational Biology

RESEARCH ARTICLE

Impact of ligand binding on VEGFR1, VEGFR2, and NRP1 localization in human endothelial cells

Sarvenaz Sarabipour[1,2*], **Karina Kinghorn**[3,4], **Kaitlyn M. Quigley**[3], **Anita Kovacs-Kasa**[5], **Brian H. Annex**[5], **Victoria L. Bautch**[3,4,6], **Feilim Mac Gabhann**[1]

1 Institute for Computational Medicine and Department of Biomedical Engineering, Johns Hopkins University, Baltimore, Maryland, United States of America, **2** Center for Cell Analysis & Modeling, Center for Vascular Biology, Department of Cell Biology, Department of Biomedical Engineering, University of Connecticut School of Medicine, Farmington, Connecticut, United States of America, **3** Department of Biology, University of North Carolina, Chapel Hill, North Carolina, United States of America, **4** Curriculum in Cell Biology and Physiology, University of North Carolina, Chapel Hill, North Carolina, United States of America, **5** Vascular Biology Center and Department of Medicine, Medical College of Georgia at Augusta University, Augusta, Georgia, United States of America, **6** McAllister Heart Institute, University of North Carolina, Chapel Hill, North Carolina, United States of America

* sarabipour@uchc.edu

OPEN ACCESS

Citation: Sarabipour S, Kinghorn K, Quigley KM, Kovacs-Kasa A, Annex BH, Bautch VL, et al. (2025) Impact of ligand binding on VEGFR1, VEGFR2, and NRP1 localization in human endothelial cells. PLoS Comput Biol 21(7): e1013254. https://doi.org/10.1371/journal.pcbi.1013254

Editor: James Gallo, University at Buffalo - The State University of New York, UNITED STATES OF AMERICA

Received: October 7, 2024

Accepted: June 20, 2025

Published: July 16, 2025

Data availability statement: All data related to this manuscript is presented in the Supporting information. The code is shared on Github at: https://github.com/SSarabipour/VEGFR-Trafficking-Projects.

Abstract

The vascular endothelial growth factor receptors (VEGFRs) bind to cognate ligands to facilitate signaling pathways critical for angiogenesis, the growth of new capillaries from existing vasculature. Intracellular trafficking regulates the availability of receptors on the cell surface to bind ligands, which regulate activation, and the movement of activated receptors between the surface and intracellular pools, where they can initiate different signaling pathways. Using experimental data and computational modeling, we recently demonstrated and quantified the differential trafficking of three VEGF receptors, VEGFR1, VEGFR2, and coreceptor Neuropilin-1 (NRP1). Here, we expand that approach to quantify how the binding of different VEGF ligands alters the trafficking of these VEGF receptors and demonstrate the consequences of receptor localization and ligand binding on the localization and dynamics of signal initiation complexes. We include simulations of four different splice isoforms of VEGF-A and PLGF, each of which binds to different combinations of the VEGF receptors, and we use new experimental data for two of these ligands to parameterize and validate our model. We show that VEGFR2 trafficking is altered in response to ligand binding, but that trafficking of VEGFR1 is not; we also show that the altered trafficking can be explained by a single mechanistic process, increased internalization of the VEGFR2 receptor when bound to ligand; other processes are unaffected. We further show that even though the canonical view of receptor tyrosine kinases is of activation on the cell surface, most of the ligand-receptor complexes for both VEGFR1 and VEGFR2 are intracellular. We also explore the competition between the receptors for ligand binding, the so-called 'decoy effect', and show that while *in vitro* on the cell surface minimal such effect would be observed, inside the cell the effect can be substantial

Funding: This work was supported by National Institutes of Health grants R01-GM129074 (FMG, BHA, VLB), R01-HL101200 (BHA, FMG), and R35-HL139950 (VLB). The funders had no role in study design, data collection and analysis, decision to publish, or preparation of the manuscript.

Competing interests: The authors have declared that no competing interests exist.

and may influence signaling. We term this location dependence the 'reservoir effect' as the size of the local ligand reservoir (large outside the cell, small inside the cell) plays an integral role in the receptor-receptor competition. These results expand our understanding of receptor-ligand trafficking dynamics and are critical for the design of therapeutic agents to regulate ligand availability to VEGFR1 and hence VEGF receptor signaling in angiogenesis.

Author summary

Receptors span the cell membrane to facilitate communication between cells and their environment. Extracellular ligands bind to these receptors and form complexes that initiate cell signaling pathways. This sensing of the environment by the receptors depends on their presence on the cell surface, however receptors move between surface and internal locations on the cell through trafficking processes. Trafficking includes production of the receptor proteins and insertion into the cell membrane; internalization via multiple pathways, recycling of intracellular receptors back to the surface, and degradation of internal receptors. Each of these processes has an impact on the receptor's presence at the cell membrane and thus the possibility to sense the environment and initiate a cellular response. The rates of these trafficking processes are different for each receptor and can be different for the ligand-receptor complexes as well. We recently developed a computational-experimental approach to quantify these processes for three important VEGF receptors; here we extend that to quantify the impact of ligand binding – specifically the binding of four members of the VEGF family – on these processes.

Introduction

Blood vessel formation is driven by sprouting angiogenesis of endothelial cells [1–3]. Angiogenesis plays a vital role in a host of physiological and pathological phenomena such as development, wound healing and tumor growth. Therapeutic induction of angiogenesis has long been a goal for ischemic diseases including peripheral artery disease and diabetes [4,5]. However, upregulating angiogenesis in patients by manipulating its key cytokine drivers, including but not limited to members of the vascular endothelial growth factor (VEGF) family, has not yet succeeded, suggesting that the system and its regulation is not yet fully understood. Thus, a more comprehensive and mechanistic understanding of the molecular drivers of sprouting angiogenesis is required for the design of effective proangiogenic molecular therapies.

The VEGF family of ligands is encoded by five human genes including VEGF-A and placenta growth factor (PLGF), which produce bivalent ligands for the endothelial cell-surface VEGF receptors (VEGFRs). The protein ligands we study here – $VEGF_{121a}$, $VEGF_{165a}$, $PLGF_1$, and $PLGF_2$ – are prominent splice isoforms of these

genes, and as constitutive antiparallel homodimers, each has two symmetric binding sites that enables the ligand to couple together two VEGFRs. We denote the VEGF isoforms here as 121a and 165a to differentiate them from the 121b and 165b isoforms [6]; $VEGF_{121a}$ and $VEGF_{165a}$ are also commonly known as $VEGF_{121}$ and $VEGF_{165}$, or VEGF-A_{121} and VEGF-A_{165}. The VEGFRs can pre-dimerize to some extent on endothelial cells in the absence of ligands [7,8], although they are not fully active in signaling until bound and dimerized by their ligands [7,9]. Upon binding of a ligand to two VEGFR1s or two VEGFR2s, the dimerized receptors trans-phosphorylate and initiate downstream signaling pathways [10–13]. $PLGF_2$ and $VEGF_{165a}$ also contain a heparin binding domain (while $PLGF_1$ and $VEGF_{121a}$ do not), enabling these ligands to bind to heparan sulfate proteoglycans (HSPGs); this domain also harbors a binding site for the VEGFR co-receptor NRP1, and so these longer isoforms can bind NRP1, which facilitates binding of $VEGF_{165a}$ to VEGFR2 and influences VEGFR2 trafficking [9,14].

VEGF and PLGF isoforms have tissue-specific expression patterns [15–19]. Each isoform likely plays specific roles due to their different receptor binding and matrix-binding profiles. For example, while expression of $VEGF_{165a}$ alone results in phenotypically normal vasculature features, $VEGF_{121a}$ results in larger, more tortuous, less branched vessels [17,20–23]. PLGF is involved in activation of macrophages that can secrete angiogenic and lymphangiogenic factors [24]. PLGF also modulates tumor angiogenesis [12,25]. However, PLGF is not required for normal murine development [26], nor for exercise-induced angiogenesis [27]. Moreover, anti-PLGF antibodies do not block primary tumor angiogenesis [28] and PLGF knockdown also does not affect endothelial cell number, migration, or tube formation in cell culture [29].

The membrane integral receptor VEGFR1 is considered a decoy receptor on endothelial cells during developmental angiogenesis [30–33]. $VEGF_{165a}$ and $VEGF_{121a}$ bind to and initiate signaling complexes with both VEGFR1 and VEGFR2 dimers, while the PLGF ligands bind to VEGFR1 but not VEGFR2. As a result, it is hypothesized that VEGFR1 binding VEGF ligands decreases the binding of those ligands to VEGFR2 and thus modulates VEGFR2 signaling. We will characterize and quantify the VEGFR1 'decoy effect' in this study. Likewise, PLGF ligand binding to VEGFR1 has been hypothesized to displace VEGF ligands from VEGFR1 and thus increase their binding to VEGFR2 and VEGFR2 signaling. A previous computational study suggested that this effect would be small [34]. Here we will quantify the potential for this effect in a more detailed model that includes receptor dimerization and much more detailed receptor trafficking. In particular, ligand-bound receptor dimers will be present both at the cell surface and on endosomes due to receptor trafficking [35–40], and thus we may observe location-specific differences in the effects of VEGFR1 and PLGF on VEGFR2 activation.

The localization of membrane-integral receptors such as VEGFR1, VEGFR2, or NRP1 is dependent on trafficking within the cell. Simply put, ligand-receptor binding requires that the ligands and receptors be in the same place at the same time. Extracellular ligands can bind to receptors on the cell surface, while intracellular ligands in endosomes can bind to receptors in those locations. In a previous combined experimental-computational study, we quantified the trafficking of VEGFR1, VEGFR2, and NRP1 in the absence of exogenous ligands [41]; here, we examine how ligand binding can alter the trafficking of these receptors. In our model, we assume that ligated and activated receptor tyrosine kinases are phosphorylated on multiple sites intracellularly, and thus can interact with different cellular components that influence trafficking pathways or rates. Capturing these differences is important because the localization of these ligand-receptor signal initiation complexes likely lead to differential downstream signaling [10,35,42].

Although the $VEGF_{165a}$ and $PLGF_1$ contributions to VEGFR2, VEGFR1 and NRP1 signaling have been studied *in vitro*, the combined effects of these ligands on VEGFR1 trafficking *in vitro* and *in silico* are not well understood. We aimed to understand the competition of VEGFR1 and VEGFR2 for VEGF binding, and the competition of VEGF and PLGF for binding to VEGFR1. The goals of this study were to: (1) elucidate the effect of $VEGF_{165a}$ and $PLGF_1$ on VEGFR1, VEGFR2, and NRP1 trafficking in human endothelial cells; (2) predict the distribution of VEGFR1, VEGFR2, and NRP1 on the cell surface and internal compartments as a function of $VEGF_{165a}$ and $PLGF_1$ treatment time and dosing; (3) investigate how this modified receptor trafficking impacts the distribution of ligated, signaling receptors; (4) compare the predicted effects of $VEGF_{165a}$ vs $VEGF_{121a}$ and $PLGF_1$ vs $PLGF_2$ to parse the effect of NRP1 binding on VEGFR1 and VEGFR2 trafficking;

(5) quantify VEGFR1's decoy effect on VEGFR2; and (6) quantify PLGF's contribution to the decoy effect. Computational models provide key insights into the combinatorial effects of multiple receptors and ligands in regulation of signaling pathways *in vitro* and *in vivo* [41,43,44]. Here, we present such measurements and modeling with specific parameters for ligand-bound receptor trafficking that are quantified here for the first time in any cell type. To our knowledge, this is the first set of VEGFR1, VEGFR2, and NRP1 trafficking experiments on the same human cell type treated with $VEGF_{165a}$ or $PLGF_1$, and the first computational model to include detailed trafficking of VEGFR1, VEGFR2, and NRP1 explicitly under ligand treatment.

Materials and methods

Computational model construction

We previously developed and parameterized a molecularly-detailed mechanistic computational model of the dynamics of membrane-integral VEGF receptors, VEGFR1, VEGFR2, and NRP1, specifically their synthesis, trafficking, and degradation in human umbilical vein endothelial cells (HUVECs) [41]. Here, we build on and extend this model to include ligand-receptor binding for four key ligands ($VEGF_{165a}$, $VEGF_{121a}$, $PLGF_1$, and $PLGF_2$), and to account for the ability of this ligand-receptor binding to alter receptor trafficking. The model includes all the reactions and parameters identified for HUVECs in our previous study, and here we estimate values for newly-added ligand-involved processes using experimental data from human endothelial cell culture.

The model uses coupled, nonlinear, deterministic ordinary differential equations describing the key biochemical and biophysical reactions including receptor-receptor dimerization (coupling), ligand-receptor binding, and trafficking of receptors and ligand-receptor complexes (Fig 1). The ligand-receptor binding and receptor-receptor coupling reactions can occur in every model compartment where the associated species are present. We use experimentally-derived surface receptor expression levels and interaction kinetics for receptors expressed in HUVECs that have been previously measured or derived, and in running the simulations we incorporate the specific geometry and initial concentrations of the *in vitro* HUVEC culture experiments being simulated.

Ligand-receptor interactions. All four of the ligands studied here bind to VEGFR1; the VEGF-A isoforms can also bind to VEGFR2 while the PLGF isoforms do not. Binding to the co-receptor NRP1 requires a NRP1-binding domain that shorter isoforms typically lack; of the ligands in our model, only $VEGF_{165a}$ and $PLGF_2$ bind to NRP1. $VEGF_{165a}$ can thus bridge VEGFR2 and NRP1 by binding to each via non-overlapping binding sites. However, this NRP1 binding is prevented when NRP1 is associated with VEGFR1 [45], perhaps due to steric hindrance, so only the shorter isoforms ($VEGF_{121a}$ and $PLGF_1$) bind to VEGFR1-NRP1 complexes, and only via VEGFR1 binding. These ligand-receptor interactions are summarized in S1 Table, and along with the receptor-receptor interactions and perhaps most crucially the receptor-to-liganded-receptor interactions (i.e., dimerization), form the basis for the many molecular complexes that can be formed (S2–S11 Tables).

Compartments. The computational model has three subcellular compartments representing different locations within the cell: the cell surface (specifically, the outward-facing portion through which receptors interact with extracellular ligands) which includes the fluid space outside the cell (i.e., culture media); early endosomes (Rab4a/Rab5a-expressing); and recycling endosomes (Rab11a-expressing). The receptors and receptor complexes move between these compartments via trafficking pathways at different rates, though we do make some simplifying assumptions to avoid an excessive number of independent parameters. The model also includes a degradation compartment, representing lysosomes or other degradative pathways, and crucially this is not included in counts of receptor numbers for the purpose of comparison to experimental results. Instead, the purpose of this compartment is to keep track of the cumulative amount of degraded receptors; the process of protein degradation in the model is represented by receptors or ligand-receptor complexes moving to the degradation compartment. We assume that the individual surface and endosomal compartments are well mixed, i.e., they are of uniform (but not constant) concentration, and we assume that receptor levels are sufficiently high to justify

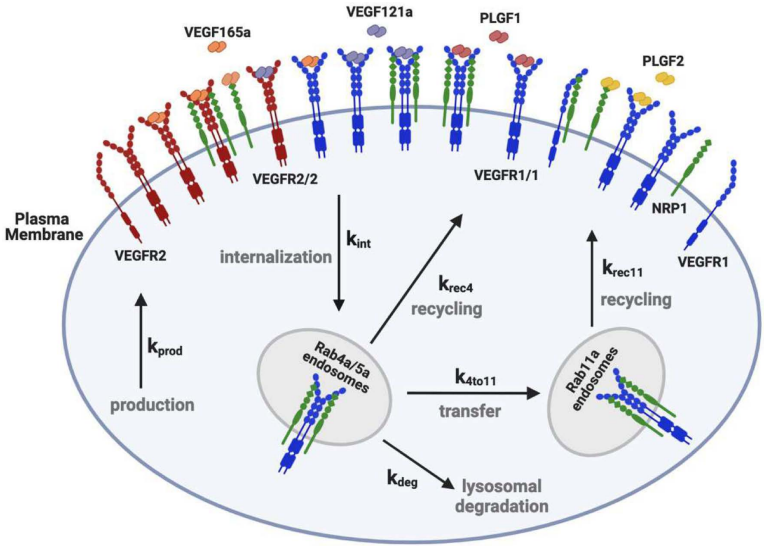

Fig 1. Diagram of molecular interactions of the computational model. Cellular biophysical and biochemical reactions between VEGFR1, VEGFR2 and NRP1 receptors, extracellular matrix components and $VEGF_{121a}$, $VEGF_{165a}$, $PLGF_1$ and $PLGF_2$ ligands. The receptors can homodimerize (at a lower level than that induced by ligands), and unlike VEGFR2, VEGFR1 can form a complex with NRP1 in the absence of ligands [45]. $PLGF_1$ binds to VEGFR1 in the absence or presence of NRP1 binding to VEGFR1. $VEGF_{165a}$ binds to VEGFR1, VEGFR2 and NRP1 and the matrix proteins. $VEGF_{165a}$ can only bind to NRP1 or matrix, not both simultaneously. $PLGF_2$ and $VEGF_{165a}$ can only bind to VEGFR1 when VEGFR1 is not bound to NRP1. $VEGF_{165a}$ can bind to NRP1 and VEGFR2 simultaneously. During trafficking, surface protein complexes (monomeric, dimeric, or higher order) can be internalized (rate constants denoted k_{int}). Early endosomal ("Rab4a/5a") receptors can be degraded (rate constant k_{deg}), recycled (rate constant k_{rec4}), or transferred to the Rab11a compartment (rate constant k_{4to11}) which leads to an additional recycling pathway (rate constant k_{rec11}). New surface receptors (monomers) are produced at rate k_{prod}. Each of the rate constant values can be different for the different receptors. Reaction rates and species concentrations are detailed in S1–S18 Tables.

https://doi.org/10.1371/journal.pcbi.1013254.g001

the continuum approximation, as previously shown [46], and thus can be represented with deterministic ordinary differential equations.

Protein synthesis and degradation. In the model, there is continual constant synthesis of new receptors to balance receptor degradation, thus representing the continuous turnover of proteins in the cell. Once synthesized, receptors are inserted into the cell surface compartment. In these simulations, ligands are added exogenously to the culture media as a step change in concentration, following a period of pre-simulation, in which the dynamics of receptor production, trafficking, and degradation proceed to steady state, to set up receptor levels on the cell surface and in the intracellular locations. Production and secretion of ligand by the cell could be incorporated, but the levels of exogenous ligand (50 $ng.ml^{-1}$ or similar concentrations, S12 Table) are sufficiently high to likely overwhelm any endogenous ligand. Receptor production rate values are identified using optimization to match the simulated cell surface receptor levels to published measurements, and the rates are given in S13 Table. The degradation of receptors and internalized ligands occurs as a first-order process from the intracellular pool.

Receptor trafficking processes. The trafficking processes, moving receptors and ligand-receptor complexes between subcellular compartments, are summarized in Fig 1, and these processes are modeled as first-order transport rates. Internalization moves surface receptors to the early endosome compartment; from these endosomes, receptors can be degraded, recycled to the surface, or trafficked to a second endosome compartment for recycling. Two recycling pathways – one via Rab4a and one via Rab11a – are included based on evidence that VEGFR2 and NRP1 use both pathways in endothelial cells [14,47]. Appropriate receptor-specific and HUVEC-specific values of the production, trafficking, and degradation rate constants for the unliganded receptors were identified in our recent study [41] and can be found in the S14 Table.

For ligand-bound receptors, the rates of trafficking may be different – as part of this study we explored the effect of multiple different ligands on VEGF receptor localization, leading to identification of a parsimonious mechanism to explain the observations (see Results). For trafficking processes that we identified to be ligand-dependent, the rate constants are different for those receptors when ligands are bound to them; if not ligand-dependent, then we assumed that the rate constants for liganded and unliganded receptors were the same. This greatly reduced the number of independent parameters needed to describe trafficking of the many receptor complexes in the system. For receptor-receptor and ligand-receptor complexes, such as VEGFR1-NRP1 or VEGFR2-$VEGF_{165a}$-NRP1, the entire complex is trafficked as a unit, the component parts do not traffic at different rates.

Receptor-receptor coupling and the impact of compartment geometry. In the absence of ligands, VEGFR1 and VEGFR2 are present as a mix of monomers and dimers due to reversible homodimerization in the absence of ligands [7,8,41]; this is in addition to the ligand-induced dimerization that will be described below. VEGFR1 and NRP1 can also bind (couple) directly to each other, while VEGFR2 and NRP1 do not; VEGFR2 and NRP1 appear to only interact when bridged by a ligand that binds both. The computational model describes the receptor levels at each location in units of #/cell (i.e., the number of molecules per cell), which makes incorporating first-order trafficking parameters simpler, and makes it straightforward to match calculated levels to experimental measurements; however, this approach impacts on the rate constants describing the receptor coupling reactions. This is described in detail in our previous work [41]; briefly, units of #/cell does not take into account the density (and therefore likelihood of interaction) of the receptors in compartments of different sizes. Assuming that the rate constants are the same on a per-surface-area basis (for two surface-associated molecules), then we can use the compartment surface areas (S12 Table) to calculate appropriate local rate constants:

$$k_{on,RR}\ \left[(\#/cell)^{-1}s^{-1}\right] = k_{on,RR}\ \left[\left(\#/\mu m^2\right)^{-1}\ s^{-1}\right]\ /\ \left(compartment\ area\ \left[\mu m^2/cell\right]\right)$$

This reduces the number of unique parameters in the model (making the model simulations more tractable). The resulting local parameter values for receptor-receptor coupling are given in S15 Table.

Ligand concentrations, ligand-receptor binding, and the impact of compartment geometry. As noted above, the units used in the model are #/cell, and therefore the concentration of the ligand added to the extracellular media (typically expressed in $ng.ml^{-1}$) is converted to #/cell using the following conversion factor using molecular weight (g/mol), the volume of fluid in the well (ml/well), and the number of cells per well (cell/well):

$$f_1 = \frac{1}{MW_L}\frac{nmol}{ng} * 10^{-9}\frac{mol}{nmol} * N_A\frac{molecules}{mol} * 1\frac{ml}{well} * \frac{1}{10^5}\frac{well}{cell}$$

Where MW_L = molecular weight of ligand ($VEGF_{165a}$, 44 kDa; $VEGF_{121a}$, 28 kDa; $PLGF_1$, 29.7 kDa; $PLGF_2$, 34.6 kDa), N_A = Avogadro's number (6.022×10^{23} molecules/mole), and thus, the values of f_1 for the four ligands are, respectively, 1.37×10^5, 2.15×10^5, 2.03×10^5, and 1.74×10^5 $\left(\frac{\#}{cell}\right) / \left(\frac{ng}{ml}\right)$.

Further, the ligand-receptor binding rate constants (k_{on} and k_{off}) must be adjusted from the standard reported form based on experimental measurements (S16 Table) to account for three things: the full dimerization model used here compared to the more common 1:1 binding model assumed to generate the parameters; to match the #/cell units of the model; and because binding can occur in each subcellular location, the volume associated with that location affects the local rate constant. The resulting parameter values are given in S17 Table. The binding rate constants are effectively one-quarter of those measured, to account for the bivalency of both ligands and receptor dimers. The unbinding rate constants are the square root of half the measured rate, to account for the two unbinding events that must occur for the ligand to fully dissociate from a dimer (for more on the derivation of these relationships, see our previous work on dimerization [48].

The binding rate constants are then adjusted using local volumes to "#/cell" units as described above for ligand concentrations, while unbinding rate constants need no adjustment due to being first order processes. As previously described [41], the endosomes enclose approximately 15 fL (about 1.5% of HUVEC volume), and assuming a 3:1 Rab4a:Rab11a split for both volume and cell surface area, this results in 11.25 fL/cell and 3.75 fL/cell for the two intracellular compartments, respectively, as compared to the 10^7 fL/cell of extracellular volume (based on 1 mL media and 10^5 cells per well; see S12 Table). As a result, the apparent (volume-adjusted) rate constants for ligands binding to receptors are much higher in endosomes than extracellularly (S17 Table), which accounts for the "#/cell" levels of ligand being concentrated in a smaller volume. It is important to have these units aligned, because the difference in size between the extracellular reservoir and the intracellular reservoir has a significant effect on ligand-receptor binding and competition.

Ligand-induced receptor coupling. Following ligand binding either to a receptor monomer or to a receptor dimer, the bivalent ligand can now bind to a second monomer or to the second receptor in the dimer. These events are related but somewhat different; binding to a second monomer is a second-order reaction involving molecules diffusing in the plane of the membrane (rate constant $k_{on,LR}$), while binding to the second receptor in a dimer is effectively an intramolecular rearrangement, and thus a first order reaction (rate constant $k_{\Delta,LR}$). We use the Δ symbol to denote that the molecule formed has three bonds – two ligand-receptor bonds and one receptor-receptor bond between the two ligand-bound receptors. The values for these rate constants are obtained as described previously [48]; briefly,

$$k_{on,LR} = \frac{(1 - k_{off,LR})}{R_{tot}}$$

Where R_{tot} is the receptor level on the surface (typically where experimental binding assays are sampling). The resulting values are then modified by surface area for the endosomal compartments (S18 Table). Comparing the receptor-receptor coupling and ligand-receptor coupling rate constants, we see that the ratio ($k_{on,RR}/k_{on,LR}$) is small (S18 Table), suggesting that ligand coupling of receptors is stronger than receptor-receptor coupling, which makes sense for ligand-induced dimerization.

Using the previously demonstrated [48] relationships that

$$k_{\Delta,LR} = (1 - k_{off,LR})$$

and

$$k_{\Delta,RR} = k_{\Delta,LR}\left(\frac{k_{on,RR}}{k_{on,LR}}\right)$$

We obtain values for these rate constants which represent, respectively, the coupling of a ligand to a second receptor in the same complex, and the coupling of two receptors that are already both bound to the same ligand (S18 Table). The similarity of the dimerization model parameterized in this way to the typical 1:1 ligand-receptor binding model can be seen in the virtual Scatchard plots generated using the models (S1 Fig). The similarity of the slopes of the lines (representing the apparent ligand-receptor affinity) and the x-intercept (apparent receptor density) indicate that the dimerization model exhibits similar ligand-binding behavior to that observed experimentally, across a range of ligand concentrations.

Pre-simulation and simulating ligand additions and perturbations. The balance of synthesis, degradation, and trafficking of receptors results in a steady-state, constant surface level of VEGFR1, VEGFR2, and NRP1 populations in the absence of ligand. These rates and steady state levels of receptors have previously been optimized and analyzed [41]. Here, we study what happens when that steady state is perturbed by ligand addition. We assume that addition of ligands is a sudden step-change in the extracellular concentration of ligands, and then use the model to simulate several hours

of experimental time. Other perturbations can be included either as sudden changes to parameter values at the time of administration (e.g., siRNA knockdown of Rab4a and Rab11a to decrease in the levels of those proteins), or as changes incorporated into the pre-simulation because they are administered long before the ligand and thus the new state of the cells must be simulated, for example receptor knockdowns.

Model solution, model outputs, and comparison with experimental data. The complete model contains 281 molecular complexes (S2–S11 Tables), including separately tracking the levels of each ligand, receptor, receptor-receptor complex, and ligand-receptor complex at each subcellular location (plasma membrane, Rab4a/5a endosomes, Rab11a endosomes) plus the degraded molecules. Code to simulate this set of 281 coupled ordinary differential equations that comprise this model was generated using the rule-based BioNetGen software; we then used the BioNetGen Visual Studio extension [49] to turn our BioNetGen model code into a MATLAB-compatible code in m-file format. This m-file encodes the molecules, reactions, and equations, and we then modified the m-file's header to function under the control of our bespoke drivers in MATLAB, for example allowing us to run simulations with different parameter values, optimization, and sensitivity analysis. The code is provided in an online repository, see *Data Availability*.

The output of the model is the concentration of each molecule or molecular complex at each location over time. To facilitate direct comparison to experimental data, the output concentrations of specific molecules or complexes are combined into aggregated quantities of interest. For example, the total VEGFR1 levels on the cell surface is the sum of all VEGFR1 in that compartment, whether in monomer form or complexed with other receptors or involved in ligand binding. If a complex contains two VEGFR1, it contributes double to the total level compared to a complex with one VEGFR1. "Internal" receptors are the sum of receptors in Rab4a and Rab11a locations; and "Total" or "Whole cell" receptors are the sum of receptors in Surface, Rab4a, and Rab11a locations. Degraded receptors are not included in any of the aggregations. Depending on the experimental measurement, e.g., levels of proteins from whole cell lysates, or only surface proteins isolated via biotin labeling, we use the appropriate aggregation of simulation results to compare to the experimental results. For predictions of 'active' molecules, i.e., receptor complexes expected to be capable of signaling, we used the sums of complexes containing a ligand that is bound to two VEGFR1 molecules or two VEGFR2 molecules.

We normalized the experimental data in the form of western blot band intensity for proteins of interest to tubulin band intensity control for equal whole cell protein loading (all proteins in the cell). We further normalized the band intensity corresponding to ligand treatment ($VEGF_{165a}$ or $PLGF_1$) conditions to the no ligand condition for each protein and experiment. For biotin-labeling experiments, the normalization is instead to PECAM (for surface receptors) or tubulin (for internal receptors) band intensity values. Since most of the experimental data is in relative units, not absolute units (exception is baseline surface receptor measurements, S12 Table), in order to compare experimental results to simulation results, we normalized the experimental data to experimental control values (no treatment conditions, or time zero condition depending on the experiment), and similarly normalized the simulation outputs described above.

Model parameter optimization. For HUVECs, we previously estimated the values of 15 receptor trafficking parameters and 3 receptor production rate parameters in the absence of exogenous ligands [41]. Rather than performing a complete additional optimization to estimate values for each of the equivalent 15 ligated receptor trafficking parameters, we expected that some of the trafficking parameters describing the movement of ligated receptors would be similar to their non-ligated counterparts. Thus, we performed simulations varying the values of trafficking rates one-by-one to identify parameters that most strongly affected model outputs, and then compared the results to experimental data for receptor localization following ligand addition. In this way we identified the most parsimonious model of how ligands impact trafficking parameters. As a result of this approach, there is sufficient data for the parameters being optimized to be identifiable (six data points to identify one parameter).

Sensitivity analysis. We performed univariate sensitivity analysis to identify parameters that most strongly affect model outputs. Key parameter values were varied as described in the text and the change in each selected output calculated. Model outputs selected included levels of expression of the receptor at the surface, inside the cell, and across

the whole cell, over time (S2–S4 Figs) in response to ligand addition. We focused on the outcomes at 60 and 240 minutes (S5 and S6 Figs) for comparison to experimental data. The sensitivity metric used is a normalized local sensitivity: percentage change in the value of the output divided by percentage change in the value of the parameter. This generally produces sensitivity values in the range of (but not limited to) negative one to plus one. A value of zero indicates no sensitivity; positive one indicates the output is linearly correlated with the parameter value; negative values indicate an inverse relationship.

Decoy effect. VEGFR1 has long been suggested to act as a decoy receptor; in other words, by binding ligand it prevents that ligand from then binding to the canonical signaling receptor VEGFR2. Functionally, this would require VEGFR1 to deplete the local ligand levels such that less ligand is available to bind to VEGFR2, since they compete for a common local pool of ligand. There is also considerable evidence that VEGFR1 is a signaling receptor in its own right, at least in adult animals [1,12,50,51]. To better understand the balance between VEGFR1's decoy role and its signaling role, it is useful to know the magnitude of the effect of VEGFR1 expression on the availability of VEGF for VEGFR2 binding. To quantify this, we created a *decoy effect* metric, expressed as the relative change in the formation of active VEGFR2 complexes due to the presence of VEGFR1. To calculate it, we simulate a scenario where VEGFR1 is absent (R1–) and compare this to a scenario with it present (R1+):

$$\textit{decoy effect} = \frac{[R2.VEGF.R2]_{R1-} - [R2.VEGF.R2]_{R1+}}{[R2.VEGF.R2]_{R1+}} \times 100$$

Expressed as a percentage, the size of this metric quantifies the degree to which the activation of VEGFR2 increases when VEGFR1 is removed; and thus reflects the amount that the presence of VEGFR1 modulates VEGFR2 activation downwards (the decoy effect). A positive value for the decoy effect metric suggests that VEGFR1 does have an impact via competition on VEGFR2 activation by VEGF, separate from any downstream signaling crosstalk effects. As with other metrics of binding and activation, the size of this decoy effect will depend on the expression and co-localization of the receptors (and of co-receptors), which are themselves dependent on the trafficking parameters; receptors cannot have an effect if they are not locally available. The above metric calculates VEGFR1's effect on VEGFR2; we calculate similar metrics to quantify the effect of VEGFR2 deletion on VEGFR1 activation, and the effect of NRP1 deletion on VEGFR1 and VEGFR2 activation.

Experimental methods

Cell culture. Human umbilical vein endothelial cells (HUVECs) were cultured at 37 °C in EBM-2 medium supplemented with a bullet kit (EGM-2) and used at passages 3–5. For each experiment, cells were used at confluence (2–3 days post-plating) (see S19 Table for manufacturers, catalog numbers, and other details of reagents).

Perturbations. Several treatments were used to inhibit specific processes in the receptor trafficking system (Fig 1). To deplete expression of recycling-associated proteins Rab4a and Rab11a in HUVECs, cells were grown to 70–80% confluency in 10 cm^2 plates and incubated with 200 pmoles of siRNA (Silencer Select Locked Nucleic Acids) and 20 μL Lipofectamine 3000 (ThermoFisher, #L3000015). Cells were transfected with control (non-targeting) siRNA duplex and siRNA duplex targeting Rab4a and Rab11a. After 48 hours, the cells were serum-starved (OptiMem + 0.1% FBS) for 18 hours, followed by ligand addition.

Whole cell protein isolation. For selected experiments, total protein expression of VEGFR1, VEGFR2, and NRP1 from whole cell lysates was measured. At appropriate time points, RIPA buffer (50 mM Tris HCl, 150 mM NaCl, 1.0% (v/v) NP-40, 0.5% (w/v) Sodium Deoxycholate, 1.0 mM EDTA, 0.1% (w/v) SDS and 0.01% (w/v) Sodium Azide) and protease/phosphatase inhibitor (Cell Signaling Technology) at a pH of 7.4 was added to the plates, lysates were collected with cell scrapers, subsequently boiled for 5 minutes at 95°C, and used for immunoblot analysis as described below. The experiments were repeated three times.

Internal and cell surface protein isolation. For other experiments, the expression of surface receptors and intracellular receptors was separated and measured via biotinylation. Biotinylation and isolation of cell surface proteins was performed according to the manufacturer's protocol (Pierce Cell Surface Biotinylation and Protein Isolation Kit, cat#A44390). Briefly, serum-starved HUVECs were washed twice in 6 ml of ice-cold PBS (Sigma-Aldrich) to stop internalization. Surface VEGFR1, VEGFR2, and NRP1 were labeled with 0.25 $mg.ml^{-1}$ of the membrane-impermeant biotinylation reagent EZ-link Sulfo-NHS-SS-Biotin (ThermoFisher Scientific) at 4°C for 30 minutes with constant rocking. The unreacted biotinylation reagent was quenched by incubation with 50 mM glycine. HUVECs were washed twice with ice-cold PBS and removed from the plate by gently scraping. After centrifugation at 800g for 5 minutes at 4°C, cells were lysed using the provided lysis buffer supplemented with protease/phosphatase inhibitors (Cell Signaling Technology). A percentage of the total lysate was reserved for total protein analysis, and the rest was put over a NeutrAvidin Agarose slurry-containing spin column (ThermoFisher Scientific) at 4°C for 1 hour. Flow-through was collected in a given volume (same for all samples), and the column was then eluted with 1 M Dithiothreitol (DTT), and the eluate was resuspended in the same volume as the flow-through, to facilitate determination of surface:internal ratios. Experiments were repeated three times.

Ligand stimulation. HUVECs were starved in EBM-2 with 0.1% serum for 12 hours prior to ligand addition. Ligand stimulation by 50 $ng.mL^{-1}$ of either Human $VEGF_{165a}$ or $PLGF_1$ (Genscript #Z02689, RnD #264-PGB-010) for 0 min, 15 min, 30 min, 60 min, 120 min and 240 min was followed by cell surface biotinylation, lysis and immunoblotting.

Immunoblots. Immunoblots were performed as previously described [52]. Briefly, whole cell lysates, or cell surface and internal fractions, were collected as described above. For whole cell lysates, approximately 10 μg of protein was separated by SDS-PAGE on 10% Tris-Acetate gels and transferred onto PVDF membranes. For biotin labeling experiments, equal volumes of the flow-through (~10 μg) and eluate were loaded to facilitate determination of surface:internal ratios. Membranes were blocked for 1 hour in OneBlock (Prometheus) and incubated at 4°C with primary antibodies (S19 Table) in OneBlock overnight. Membranes were washed 3 times in PBST (PBS 0.1% Tween-20) before adding HRP-conjugated secondary antibodies for 1 hour at room temperature. Secondary antibodies were removed, and membranes washed four times in PBST before addition of Luminata Forte (Millipore). See S19 Table for details of antibodies, inhibitors and siRNAs used for this study. BioRad software was used to image the western blots, and ImageJ software was used to isolate and quantify the specific bands produced by the antibody. Loading control (typically α-tubulin) was used to normalize the amount of total protein present.

Statistics. Experimental data was analyzed using single factor analysis of variance (ANOVA) across multiple groups (e.g., surface receptor levels under ligand treatment at different time points). Significance levels were calculated using t-test ($p < 0.05$) with correction.

Results

Impact of $VEGF_{165a}$ and $PLGF_1$ on VEGF receptor trafficking in HUVECs

We previously estimated the values of 15 receptor trafficking parameters and 3 receptor production rate parameters in the absence of exogenous ligands in HUVECs [41]. To study the impact on receptor trafficking of $PLGF_1$ binding to VEGFR1 and $VEGF_{165a}$ binding to VEGFR1, VEGFR2, and NRP1, we measured whole-cell expression levels of VEGFR1, VEGFR2, and NRP1 in HUVECs following addition of these exogenous ligands. Cells were serum starved for 12 hours, then treated with 50 $ng.mL^{-1}$ of $VEGF_{165a}$ or $PLGF_1$ for 15 min, 30 min, 1 hr, 2 hr, and 4 hr, and compared to the no-ligand-added case. Over time, we did not observe consistent changes in whole-cell levels of VEGFR1 or NRP1 under treatment with either ligand (Fig 2A–D). Whole-cell VEGFR2 levels seemed lower at later times (down 42% and 31% after 2 hours and 4 hours) following $VEGF_{165a}$, but with high variability between replicates (Fig 2A and 2C); there was no similar response to $PLGF_1$ (Fig 2B and 2D).

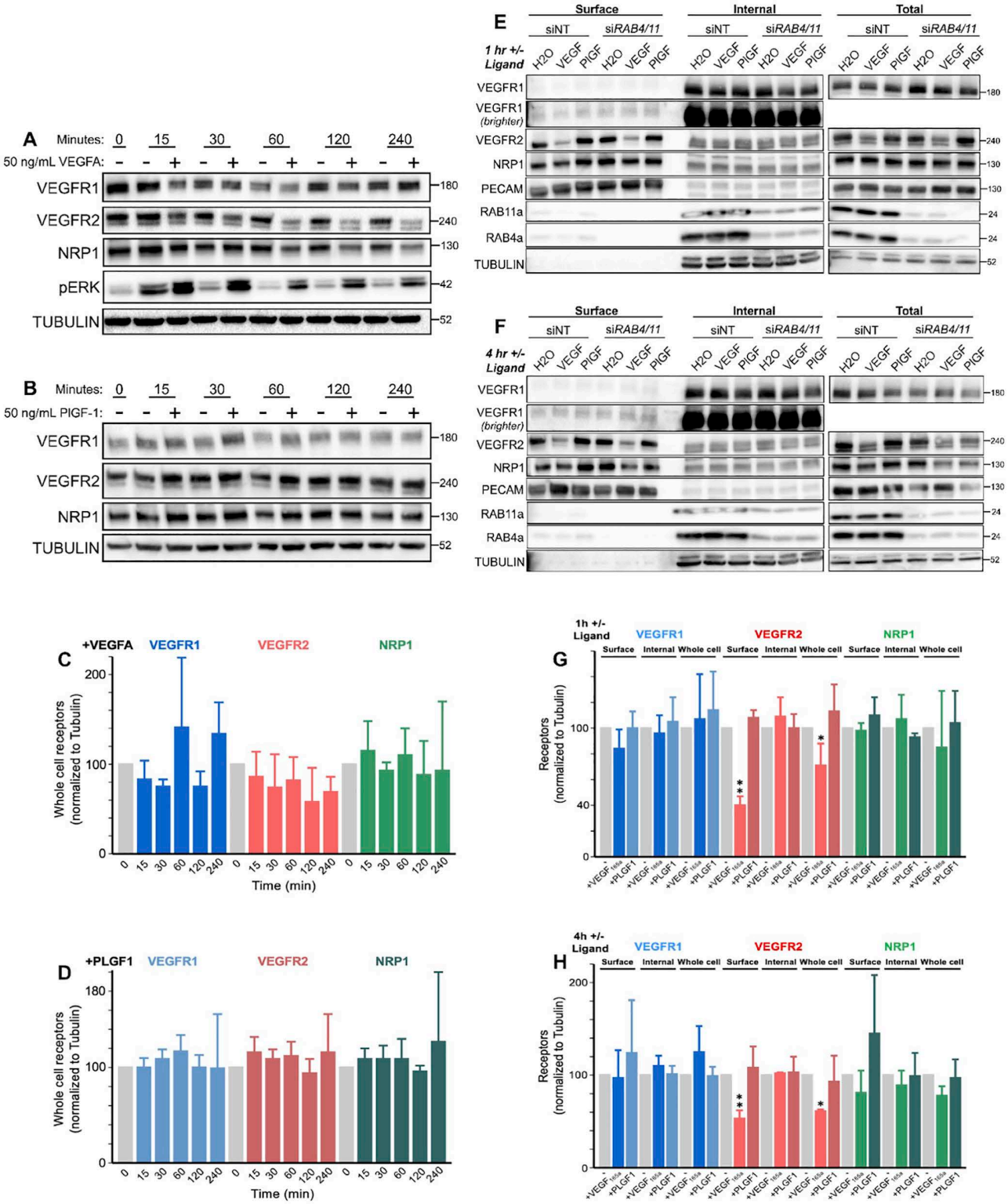

Fig 2. Experimental measures of whole-cell and surface levels of VEGFR1, VEGFR2, and NRP1 in HUVECs. A, B, Western blot of total HUVEC lysates treated as indicated for 0.25–4 hours with 50 μg.mL^{-1} of VEGF$_{165a}$ (A) or PLGF$_1$ (B) and stained for VEGFR1, VEGFR2 and NRP1. Representative of n = 3 replicates. C, D, Quantification of whole cell receptor levels shown in A,B. E, F, Western blot of Biotin labeling assay to measure surface

and internal VEGFR1, VEGFR2, and NRP1 levels in HUVECs; for 1 hour and 4 hours with 50 μg.mL^{-1} of $VEGF_{165a}$ or $PLGF_1$ and stained for VEGFR1, VEGFR2 and NRP1. Representative of n = 3 replicates. Western blot showing the effect on VEGFR1, VEGFR2 and NRP1 levels of depletion of both Rab4a and Rab11a for 1 hour and 4 hours ligand treatment; Representative of n = 3 replicates. Control conditions in E and F include nontargeting siRNA (siNT). Reagents used for the experiments are detailed in S19 Table. G, H, Quantification of whole cell receptor levels shown in E, F. The trend of reduced whole cell VEGFR2 following $VEGF_{165a}$ administration observed in A and C is consistent with significant differences (by single factor ANOVA analysis, *, $p < 0.01$; **, $p < 0.0001$) for surface and whole cell VEGFR2 levels at 1 hour and 4 hours post-$VEGF_{165a}$ addition compared to no ligand addition, observed in E-H.

https://doi.org/10.1371/journal.pcbi.1013254.g002

We previously showed that whole-cell receptor expression does not tell the full story; quantifying changes to receptor levels in different cellular compartments can reveal trafficking. To quantify receptor levels in the cellular compartments, we used surface biotin labeling to separate and quantify the surface and internal pools of NRP1, VEGFR2, and VEGFR1 in the absence and presence of ligands. Surface biotinylation labeled total surface proteins on serum-starved HUVECs, and these labeled proteins were then captured on streptavidin beads. We then used western blotting to quantify the levels of surface (biotinylated) and intracellular (non-biotinylated) NRP1 in the absence of trafficking perturbations (Fig 2E–2H, *siNT*). From this, we can see that surface VEGFR2 levels decrease following $VEGF_{165a}$ treatment and stay decreased over time, consistent with other published observations of VEGFR2 decreases following ligand addition [1,2]. Interestingly, the internal receptor levels do not increase to compensate; any increase is slight, not significant, and transient; and the total receptor levels are decreased (but by a lesser amount than the surface VEGFR2). By contrast, VEGFR1 and NRP1 levels, both on the surface and intracellularly, were not significantly changed by either $VEGF_{165a}$ or $PLGF_1$ treatment; and VEGFR2's surface and internal levels were also unchanged by $PLGF_1$.

Given the involvement of Rab4a and Rab11a in recycling (Fig 1), we also explored the effect of Rab4a and Rab11a knockdown via siRNA on receptor expression following ligand treatment (siRNA was administered 18 hours before the ligand addition, to allow time for the knockdown of Rab4a and Rab11a proteins (Fig 2E and 2F). These knockdowns did not substantially affect localized receptor expression levels.

Moving to the computational model, we explored potential explanations for the experimentally-observed temporal differences in localized VEGFR2 levels. We first explored increased internalization of $VEGF_{165a}$-bound VEGFR2 (compared to unligated VEGFR2), because this is one of the known effects of VEGFR2 activation, typically understood to be due to enhanced association of phosphorylated VEGFR2 with clathrin internalization pathways [3–10]. Testing different levels of increase to the internalization rate constant, we found that the lower surface levels of VEGFR2 are consistent with ligand-activated VEGFR2 having an internalization rate constant three times that of unactivated VEGFR2 (Fig 3A). As validation, we also compared the simulation-predicted impact of ligand binding on the intracellular and whole cell VEGFR2 levels to our experimental measurements (Fig 3B and 3C respectively), and these were consistent; we found that the transient increase in internal VEGFR2 levels and decreased whole cell VEGFR2 levels are recreated by the same parameter change. At first, the transient internal VEGFR2 change was somewhat surprising; since the increased internalization depletes VEGFR2 surface levels, we might expect compensatory increased internal VEGFR2 levels. However, what the model suggests is happening is that the increased internalization briefly increases the internal levels, but then degradation returns the internal VEGFR2 to pre-ligand levels. The model predicts this transient behavior without any change to the intrinsic degradation rate constant; rather, the higher VEGFR2 levels themselves increase the rate, and the driver for internal steady state levels (both before ligand and after ligand) is the balance of receptor production (assumed not to change) and degradation. Thus, the internal levels have to return to pre-ligand levels even with the increased internalization. This kind of nonobvious mechanistic insight is part of why experimental-computational combined approaches are powerful.

Among the various trafficking parameters, degradation was the only other parameter to which VEGFR2 levels were sensitive in our previous ligand-free study [41], because VEGFR2 recycling was not quantitatively important. Thus, we checked whether, along with or instead of VEGFR2 internalization, ligand-modified VEGFR2 degradation rate constants could explain the observations; however, altering the degradation rate constant did not affect surface VEGFR2 levels (Fig

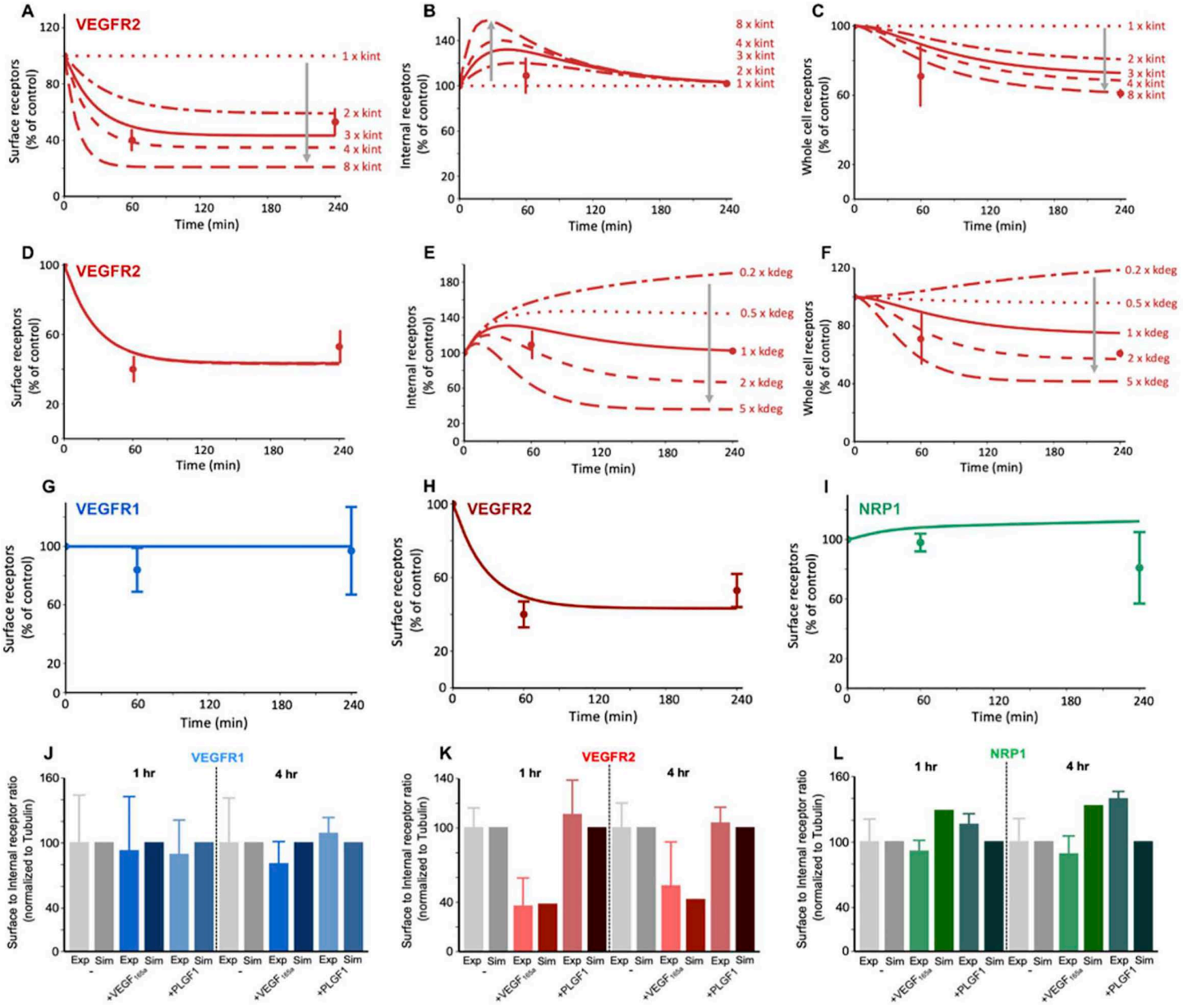

Fig 3. Ligand treatment - here, $VEGF_{165a}$ - alters VEGFR2 distribution but not VEGFR1 or NRP1 distribution. A-C, total (ligated and unligated) receptor levels on the cell surface, inside the cell, and combined (whole cell) following $VEGF_{165a}$ treatment. The experimentally-observed decline in surface and whole cell levels, simultaneous with a stable internal level, is consistent with a VEGF-induced three-fold increase in VEGFR2 internalization (V.R2.kint), compared to the unligated receptors, lines represent 8x, 4x, 3x, 2x, 1x, D-F, total (ligated and unligated) receptor levels on the cell surface, inside the cell, and combined (whole cell) following $VEGF_{165a}$ treatment. Using the increased VEGFR2 internalization as a baseline, changes to ligand-induced degradation of VEGFR2 (V.R2.kdeg) do not improve the fit to experimental observations, lines represent 5x, 2x, 1x, 0.5x, 0.2x, G-I, the simulated results with enhanced VEGFR2 internalization shows a match between the predicted and experimentally changes in surface receptor levels for VEGFR1, VEGFR2, and NRP1. J-L, Experimental and simulated surface to internal ratios for VEGFR1, VEGFR2 and NRP1 in the absence of ligands and under 1h and 4h ligand treatment conditions (normalized to the unligated values). See S2–S7 Figs.

https://doi.org/10.1371/journal.pcbi.1013254.g003

3D), and thus could not explain those levels, and furthermore it resulted in long-term changes to internal and whole cell VEGFR2 levels (Fig 3E and 3F), and thus could not explain those observations either. Altering the recycling rate constants for ligand-bound VEGFR2 did not affect VEGFR2 levels at any location S2G–S2O Fig), as expected because VEGFR2 recycling rate constants are very low (S14 Table) and little VEGFR2 is recycled [41]. Our simulation results with enhanced VEGFR2 internalization show a match between the predicted and experimentally changes in surface receptor levels for VEGFR1, VEGFR2, and NRP1 (Fig 3G–3I).

Simulating the potential impact of ligands on VEGFR1 trafficking (S3 and S4 Figs) has some similarities and some differences to VEGFR2. For example, like VEGFR2, increased internalization would decrease surface VEGFR1 (S3A and S4A Figs), but it would have even less impact on internal and whole cell VEGFR1 than on VEGFR2, because most of VEGFR1 is already internal [41]. Ligand-induced alterations to the degradation rate of VEGFR1 would be predicted to impact both surface and internal levels of VEGFR1 (S3D–F and S4D–F Figs); increased degradation lowers internal levels, which decreases the number of receptors available for recycling to the surface. That's different from VEGFR2, for which the surface level depends only on production and internalization, because recycling is low in these cells. Increasing recycling rates increase surface VEGFR1 levels (though the second step of Rab11a-recycling is not the bottleneck and therefore sees no change (S3M–O Fig)).

To explore this more systematically, we performed simulations varying the values of individual trafficking rate constants and evaluated receptor levels at each location, to identify parameters that most strongly affected model outputs (S5 and S6 Figs). Since we know that in the experiments we didn't observe substantial changes to whole cell, surface, and internal levels of either VEGFR1 or NRP1, we assumed that the trafficking rate constants for these receptors - at least those that in simulations result in changes to the observed metrics - are unaffected by ligand binding. We should note, however, that because the amount of VEGFR1 on the surface is already low (10% or less of cellular VEGFR1; [41]), the effect of changes to the internalization rate constant for VEGFR1 (S4 Fig) may not show up in experimental data - first, because the impact on surface VEGFR1 would be to deplete an already hard-to-measure low level; and second, because the effect on internal and whole cell VEGFR1 is so small (even smaller than the effect for VEGFR2). Therefore, we proceed with an assumption that VEGFR1 internalization rate is not affected by ligand binding, and while we can't rule out that this may be incorrect, if it is then the level of effect on the already-skewed VEGFR1 localization is expected to be negligible. Overall, the picture that emerges is that there are no trafficking alterations by ligand binding needed to match the observations for VEGFR1 or NRP1, and thus the most parsimonious and consistent conclusion is that only the internalization of VEGFR2 is affected, as evidenced by its effects on VEGFR2 levels and their consistency with experimental data (Fig 3).

As another way of looking at these trafficking changes, we calculated the overall transport rates (i.e., rate constant multiplied by concentration) for the receptors moving between subcellular locations (S7 Fig). The overall rates of VEGFR1 movement are higher than VEGFR2 but are unaffected by ligand addition (Fig 3J). VEGFR2 internalization and degradation are transiently increased (1 hour, S7E and S3K Figs) until a new steady state is established with different receptor localization (4 hours, S7H and S3K Figs). Ligand addition also has an impact on NRP1 trafficking rates as NRP1 coupling to VEGFR2 via the ligand will exhibit slower transport than NRP1 coupled to VEGFR1 (S7C, S7F and S7I Fig). However, overall trafficking remains balanced and the levels of NRP1 in different locations are not predicted to change substantially (Fig 3I and 3L), which matches the experimental measurements (Figs 2, 3I and 3L).

As additional validation of the model, we simulated disruption to the Rab4a/Rab11a recycling pathways (S8 Fig) and compared it to experimental siRNA-mediated knockdown of both Rab4a and Rab11a in HUVECs (Fig 2E–H). Expression of VEGFR1, VEGFR2, and NRP1 was measured following siRNA-Rab4a/siRNA-Rab11a treatment, in the absence and presence of 50 $ng.mL^{-1}$ of $VEGF_{165a}$ or $PLGF_1$ at 1 hour and 4 hour timepoints following knockdown and serum starvation to assess changes to stability/turnover. The surface, internal or whole-cell levels of VEGFR1, VEGFR2, and NRP1 were essentially unaffected by Rab4a/11a knockdown experiments (Fig 2E and 2F) and in the equivalent simulations (S8 Fig), receptor stability in response to ligands was similarly unaffected by the Rab4a/Rab11a knockdown.

Impact of receptor trafficking on ligand-induced receptor activation

To this point we have focused on receptor localization, counting both ligated and unligated receptors. Signaling is generally initiated by ligated, activated receptors, and thus we explored how trafficking of the three different receptors might result in different localized levels of active receptors. This differential localization of active receptors is important, given previous studies supporting the concept that signal initiation in different subcellular locations can result in activation of different signaling pathways and different cell behaviors [53–58].

We define active VEGFR1 and VEGFR2 as being in complexes where two receptors are bound to the same bivalent ligand (receptor-ligand-receptor complexes). Activation of receptors may have additional complexity, including the differential localization of phosphatases that can site-selectively dephosphorylate tyrosines in the intracellular domains of the receptors, but here we focus on the potential for ligand-induced receptor activation by location. We simulated four ligands: $VEGF_{165a}$ and PLGF1 based on the experimental data, plus $VEGF_{121a}$ and $PLGF_2$ using the same trafficking rates as their isoforms but reflecting the distinct receptor-binding capabilities as described earlier (S1 Table).

VEGFR2 on the surface of the cells first encounters ligands that are outside the cell, and on binding forms signal-capable complexes; as these complexes internalize faster than other VEGFR2, these complexes then decline over time (Fig 4A). The active complexes moved inside (Fig 4B), and ultimately more signal-capable complexes are present inside the cell than on the surface of the cell (Fig 4A–C), in contrast to the initial 50–50 distribution of VEGFR2 between the cell surface and inside the cell. Signal-capable complexes decline over time, but slowly, as degradation inside the cell is mostly balanced by new receptor production, and there is a plentiful supply of ligands in the extracellular media to bind to these new receptors. The apparent higher activation of VEGFR2 by $VEGF_{121a}$ vs $VEGF_{165a}$ is largely due to higher initial molar ligand concentrations (in nM) for the same weight-based concentrations (in ng/ml) as $VEGF_{121a}$ has a lower molecular weight (S12 Table).

As for VEGFR1, we know that the expression of the receptor on the surface is very low, and as a result few active receptor complexes are formed (Fig 4D). The question then is, with the great majority of VEGFR1 inside the cell, whether a sufficient ligand can internalize and ligate those receptors? Clearly, the answer is yes (Fig 4E). The exchange on VEGFR1 via internalization and recycling is sufficient to bring ligated receptors into the cell where they account for the vast majority of the ligated VEGFR1 across the whole cell (Fig 4D–F). We considered that perhaps ligands enter the cell via binding the more numerous surface VEGFR2 and then rebinding to internal VEGFR1 once inside the cell, and likely this does contribute, but it is not required, as $PLGF_1$ binds only to VEGFR1 (S1 Table) yet shows significant internal ligation (Fig 4E). $PLGF_2$ is predicted to induce less activation than $PLGF_1$, largely due to inability to bind the R1-N1 complex (S1 Table).

The bias towards intracellular active receptor complexes is illustrated more clearly when compared side-by-side after 1 hour (Fig 5A) and 4 hours (Fig 5B) of ligand stimulation. Another consequence active receptor internalization is that ligands can unbind from (and rebind to) receptors while inside the cell, resulting in the presence of free (unbound) ligands inside endosomes (Fig 5C and 5D) and a different equilibrium between ligands and receptors inside the cell than pertains at the cell surface.

We also ran simulations across a range of extracellular ligand doses, showing similar observations across the range of concentrations - e.g., higher surface VEGFR2 activation at earlier times and decrease at later times (S9 Fig), and high levels of internal VEGFR1 activation (S10 Fig). At lower concentrations, $VEGF_{165a}$ has an advantage over $VEGF_{121a}$ in VEGFR2 activation due to its ability to bind to NRP1 (S9 Fig), while at higher concentrations, as receptors get saturated, $VEGF_{121a}$ becomes a more potent inducer of VEGFR2. $VEGF_{121a}$ is predicted to induce higher VEGFR1 activation than $VEGF_{165a}$ (S10 Fig), due to the high levels of NRP1-VEGFR1 heterodimers, which permit binding of $VEGF_{121a}$ but not $VEGF_{165a}$ (S1 Table). For similar reasons, $PLGF_1$ is predicted to be a stronger inducer of VEGFR1 than $PLGF_2$ (S10 Fig). An alternate illustration of both the dose-dependency and the internal bias is shown in S11 and S12 Figs.

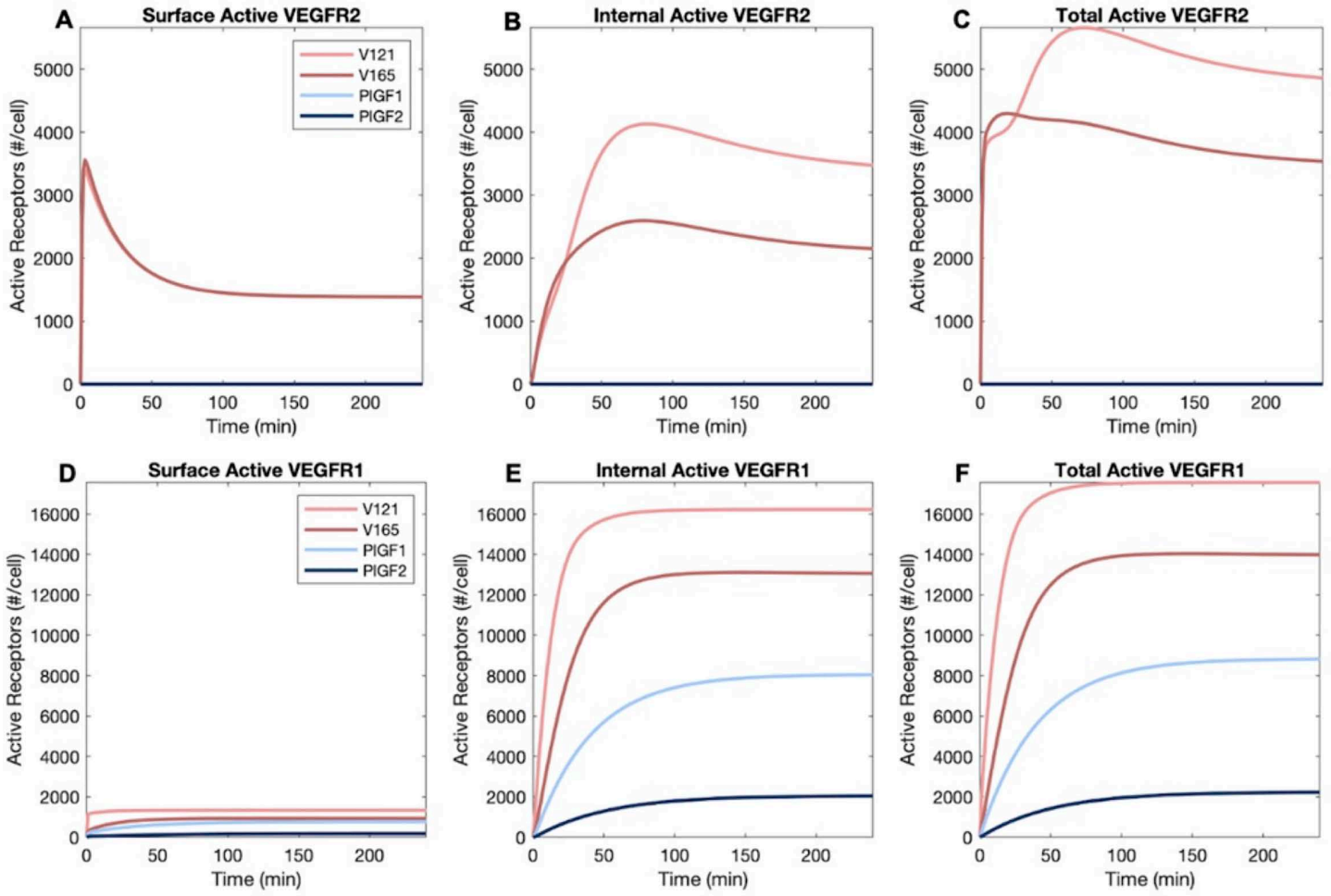

Fig 4. Distribution of ligated and active VEGFR1 and VEGFR2 receptors following addition of one ligand. A-C, Cell surface (A), internal (B), and whole cell (C) VEGFR2 following 50 ng.ml^{-1} $VEGF_{121a}$ or $VEGF_{165a}$, D-F, cell surface (D), internal (E), and whole cell (F) VEGFR1 following 50 ng.mL^{-1} $VEGF_{121a}$, $VEGF_{165a}$, $PLGF_1$ or $PLGF_2$. V165 represents $VEGF_{165a}$, V121 represents VEGF121a, P1 represents $PLGF_1$, and P2 represents $PLGF_2$.

https://doi.org/10.1371/journal.pcbi.1013254.g004

One notable feature of the ligand dose-dependence curves (S9 and S10 Figs) is that at high concentrations, there is a dip in several of the curves, i.e., increasing the added ligand concentration further decreases receptor ligation and activation. This phenomenon can also be seen when exploring the dimerization of receptors (S13 Fig): in the absence of exogenous ligands, some VEGFR1 and VEGFR2 are dimerized (though inactive). As ligands are added, at low ligand concentrations, ligands bind receptor monomers (or bind to receptor dimers but only once) not increasing dimerization; then at intermediate concentrations, dimerization increases alongside activation; and at higher ligand levels, receptor monomers become saturated with bivalent ligand and increased ligand binding decreases dimerization. The heterodimers formed by VEGFR1 and NRP1 exhibit only slightly increasing prevalence in the presence of ligands that bind the heterodimers (S14 Fig), while they decrease at higher concentrations of ligands that do not (e.g., $VEGF_{165}$).

Decoy effects and the impact of competition. As noted earlier, VEGFR1 may have both intrinsic signaling function and modulate VEGFR2 signaling via decoy function. This 'decoy effect' is due to competition for ligand binding; ligands that bind VEGFR1 decrease the available pool of ligands for binding to VEGFR2. To quantify the likely size of the decoy effect, we predicted the number of active ligated VEGFR2 induced by $VEGF_{165}$, both with and without the presence

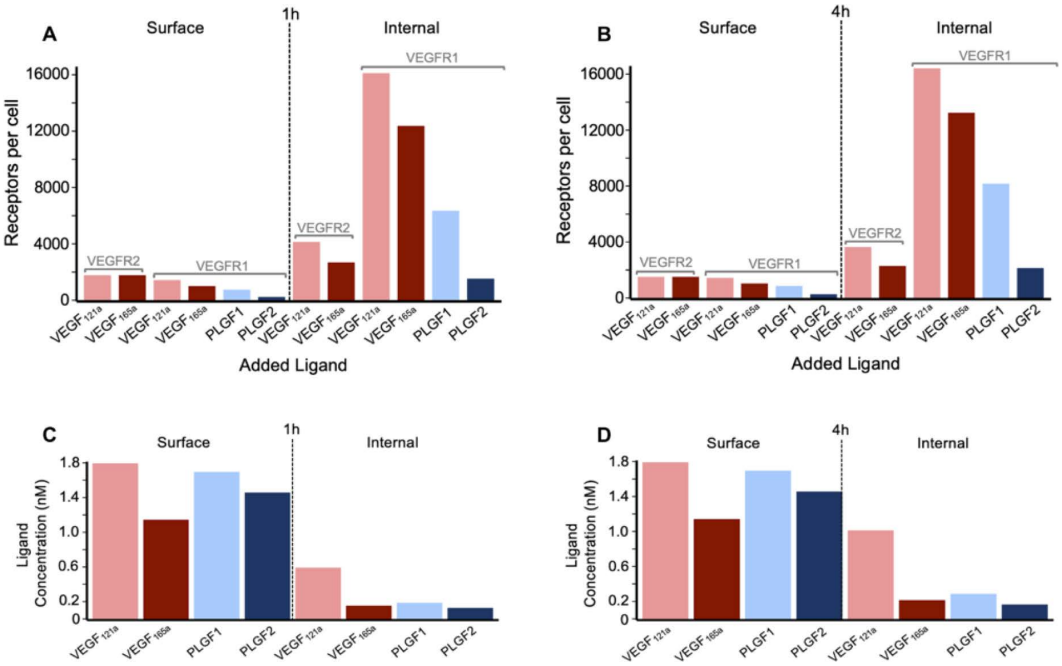

Fig 5. Distribution of ligands and of active ligated VEGF receptors. A, B, Levels of active VEGFR1 and VEGFR2 on the cell surface and internally, following 1 hour (A) or 4 hour (B) treatment with 50 ng.mL^{-1} of $VEGF_{165a}$, $VEGF_{121a}$, $PLGF_1$, or $PLGF_2$. C, D, Concentration of extracellular ligand ("surface") and intracellular ligand ("internal") following 1 hour (C) or 4 hour (D) treatment with 50 ng.mL^{-1} of $VEGF_{165a}$, $VEGF_{121a}$, $PLGF_1$, or $PLGF_2$. See the dose-dependent impacts on these levels in S13 and S14 Figs.

https://doi.org/10.1371/journal.pcbi.1013254.g005

of VEGFR1. In this way, we estimated the size of VEGFR1's decoy effect on VEGFR2, the calculations for which are described in *Methods*.

Aggregating across the whole cell, in the presence of VEGFR1 (Fig 6A) increasing VEGF levels result in higher levels of VEGFR2 signal-initiation complexes, resulting in thousands of active VEGFR2 per cell. The early peak and partial decline over time is also visible. Without VEGFR1 (Fig 6B), the same patterns are present, however the overall level of active VEGFR2 is higher; the removal of VEGFR1 appears to have freed up ligand that now can bind to and activate VEGFR2. The net effect of this is strongest at lower VEGF concentrations (Fig 6C); this makes sense, as (a) the higher the VEGF concentration in the media, the smaller the impact that VEGFR1 binding has on VEGF concentration, and consequently on the binding to VEGFR2; and (b) at higher concentrations, VEGFR2 is already close to saturation and so additional ligand will not add many additional active complexes.

However, we previously explored this decoy effect, with a model of VEGFR1-VEGFR2 competition that had less detail on receptor trafficking [34,44,59], that predicted minimal decoy effect, and little impact of VEGFR1 on VEGFR2 ligation. So why the difference? In the previous work, receptors were only present on the cell surface; they could be dynamically produced and internalized but were considered degraded once inside the cell. In this updated model with detailed trafficking, we can separate out the effects of VEGFR1 on VEGFR2 on the surface (Fig 7C) and inside the cell (Fig 7F). What we see is entirely consistent with that previous work - on the surface, there is essentially no decoy effect. This is not just because the VEGFR1 is present at lower levels on the surface than inside the cell (Fig 7A and 7B), though that may contribute slightly; the real distinction here is that the cell surface receptors are facing out into a large reservoir of ligand in the extracellular media. Even if the concentrations are similar outside the cell and in endosomes, the difference in volume between the two locations is crucial. VEGFR1 on the surface binding VEGF results in very little decline in the

Fig 6. Impact of VEGFR1 on whole cell VEGFR2 ligation by VEGF$_{165a}$. A, changes in VEGFR2.VEGF$_{165a}$.VEGFR2 levels under varying VEGF$_{165a}$ concentrations B, changes in VEGFR2.VEGF$_{165a}$.VEGFR2 in the absence of VEGFR1 levels under varying VEGF$_{165a}$ concentrations C, percent change in VEGFR2.VEGF$_{165a}$.VEGFR2 levels under loss of VEGFR1 molecules and under varying VEGF$_{165a}$ concentrations. When VEGFR1 is removed, whole cell VEGFR2.VEGF$_{165a}$.VEGFR2 levels change.

https://doi.org/10.1371/journal.pcbi.1013254.g006

overall concentration extracellularly because, relatively, there is so much ligand available in the large extracellular volume. By contrast, VEGFR1 binding VEGF inside the cell can significantly deplete VEGF concentration in endosomes because the actual amount of VEGF there (amount = concentration times volume) is lower. And thus, the decoy effect can be seen to be a phenomenon of intracellular receptors (Fig 7F) rather than surface receptors, with a major impact on intracellular VEGFR2 activation at all but the highest (already saturating) ligand concentrations (Fig 7D–F). We introduce the term 'reservoir effect' to describe this impact that the size of the available ligand reservoir has on the decoy effect. The total available ligand reservoir (concentration times volume) being larger means that the impact of receptor binding on that ligand's concentration is smaller; whereas for smaller reservoirs (typical of smaller volumes, e.g., inside vesicles), the effect on ligand concentration can be much larger.

As noted earlier, NRP1 is a co-receptor for some VEGF/PLGF isoforms and not others (S1 Table) and leads to impacts on the binding of different ligands to the receptor tyrosine kinases and their resulting activation (Figs 4 and 5). This can be seen to be a ligand-dose-dependent effect (S9 and S10 Figs) that is stronger at lower ligand levels. We computationally deleted NRP1 and calculated the impact on VEGF$_{165a}$ activation of VEGFR2 (S15–S17 Figs) and VEGFR1 (S18–S20 Figs). Indeed, the loss of NRP1 causes a sizable decrease in VEGFR2 activation at lower concentrations, due

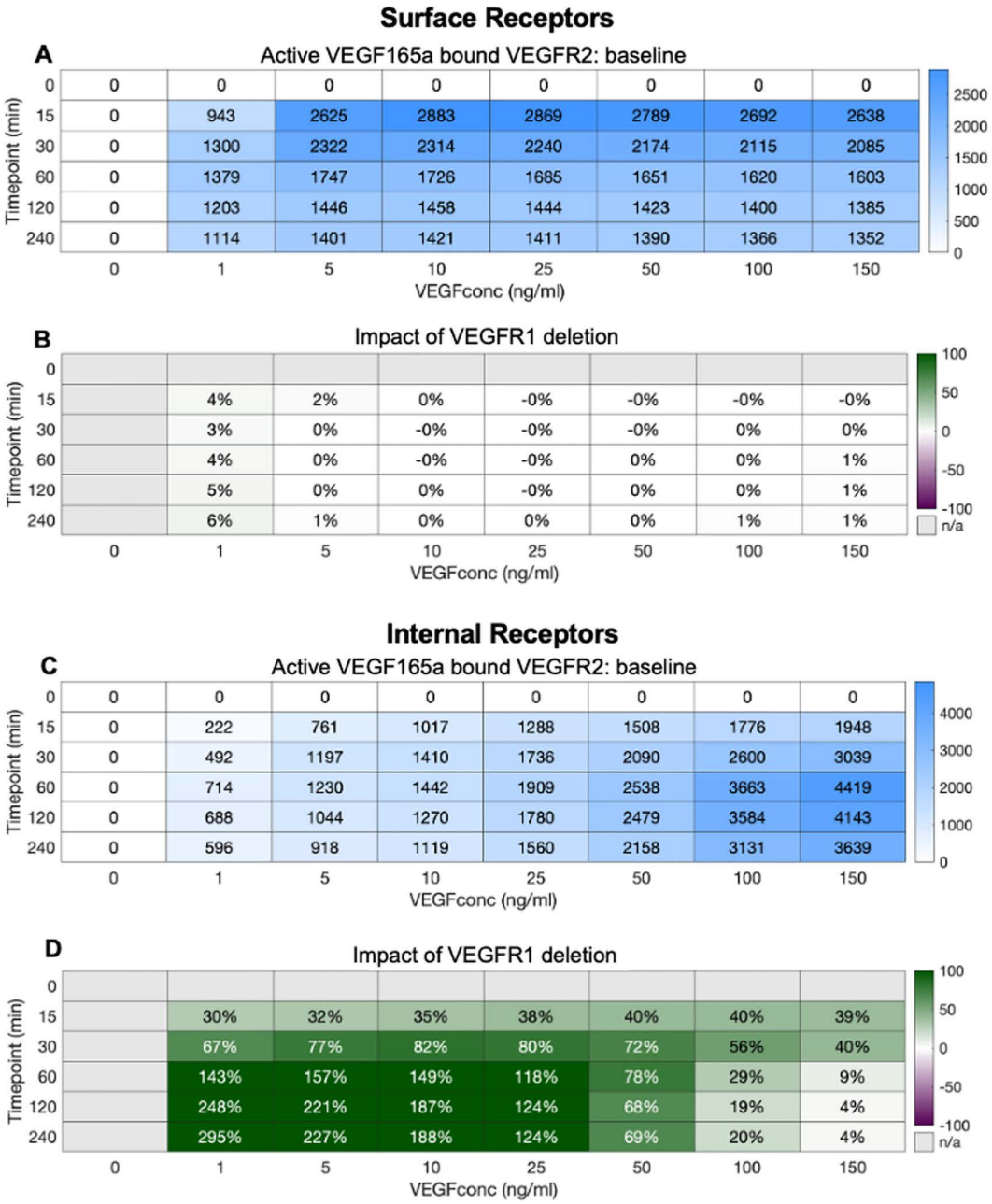

Fig 7. Impact of VEGFR1 on A,B, Surface and C,D, Internal VEGFR2 ligation by VEGF$_{165a}$. Changes in VEGFR2.VEGF$_{165a}$.VEGFR2 levels under varying VEGF$_{165a}$ concentrations. Change in VEGFR2.VEGF$_{165a}$. VEGFR2 levels under loss of VEGFR1 molecules and under varying VEGF$_{165a}$ concentrations. When VEGFR1 is removed, surface VEGFR2.VEGF$_{165a}$.VEGFR2 does not change but internal VEGFR2.VEGF$_{165a}$.VEGFR2 levels change over a range of VEGF$_{165a}$ concentrations.

https://doi.org/10.1371/journal.pcbi.1013254.g007

to the loss of the avidity provided by the VEGFR2-VEGF-NRP1 complexes. At higher ligand concentrations, there is a small but opposite effect, likely due to the ligand coming close to saturating the receptors, and the removal of NRP1 now eliminating a large sink for ligand binding. There are slight quantitative differences in these effects on the cell surface (S16 Fig) vs internally (S17 Fig) due to different relative levels of the receptors in these locations, but the trends are the

same. By contrast, $VEGF_{165a}$ activation of VEGFR1 is strongly enhanced by NRP1 deletion (S18–S20 Figs), because the VEGFR1-NRP1 heterodimers are no longer formed, making VEGFR1 more available for $VEGF_{165a}$ binding. This effect is stronger at lower ligand concentrations, again because at higher concentrations the barriers to binding are more easily overcome. Putting these insights together, we can see that the presence of NRP1, at low or moderate concentrations, would be expected to enhance binding to VEGFR2 and diminish binding to VEGFR1 - both elements pushing the system in the direction of more VEGFR2 signaling. Of note, at higher ligand concentrations typical of *in vitro* studies (such as 50 ng/ml), the impact of NRP1 is much smaller; however, concentrations *in vivo* are typically considerably lower than those used *in vitro* [6], and thus we might expect NRP1 to have a more sizeable effect *in vivo*.

Just as we have seen the impact of VEGFR1 on VEGFR2 activation, there can be a reciprocal impact of VEGFR2 on VEGFR1 ligand binding and activation (S21–S23 Figs). Again, we see a stronger effect of VEGFR2 on VEGFR1 at lower ligand concentrations, but perhaps surprisingly, while VEGFR1 deletion increases VEGFR2 activation (Figs 6 and 7), loss of VEGFR2 is predicted to decrease activation of VEGFR1. This holds both on the surface (S22 Fig) and inside the cell (S23 Fig). The effect of VEGFR2 on VEGFR1 is also due to the presence of NRP1. The presence of VEGFR2 allows the formation of VEGFR2-VEGF-NRP1 complexes, which reduces the formation of VEGFR1-NRP1 complexes that prevent the binding of $VEGF_{165}$. Thus, with VEGFR2 deleted, VEGFR1-NRP1 complexes dominate and $VEGF_{165a}$ binding to VEGFR1 is lower.

Having quantified the effects of receptors competing for ligand binding, we can also quantify the effects of ligands competing for receptor binding. Specifically, PLGF and VEGF both bind to VEGFR1. Our simulations thus far manipulated one ligand at a time, and under these conditions PLGF exhibits time- and dose-dependent activation of VEGFR1 (S24 Fig). However, tissues often express multiple isoforms, so we explored co-administration of two ligands (Figs 8 and S25–S28). Unlike receptors, where competition was higher at low ligand concentrations, these simulations reveal that competition is higher at high ligand concentrations, likely because at these high levels depletion of available free receptors leads to the competition effects. For example, at 5 ng/ml of both $VEGF_{165a}$ and $PLGF_1$, VEGF-bound active VEGFR1 is reduced only 3.7% by the addition of PLGF1 (Figs 8B and S25), while this raises to 20% and 23% at 50 ng/ml and 150 $ng.ml^{-1}$, respectively. $VEGF_{165a}$ has a much stronger effect on $PLGF_1$; VEGFR1 activated by PLGF is reduced 15%, 50%, and 68% for initial ligand concentrations of 5, 50, and 150 $ng.ml^{-1}$ (Figs 8C and S26). Unlike competition by receptors for ligands, competition by ligands for receptors is not primarily mediated by changes to ligand levels (S27 Fig), which reflects saturated binding (and the scarcity of unligated receptors) as the key mediator. What about the consequences of VEGF-PLGF competition on VEGFR2 activation? PLGF cannot bind VEGFR2, but if PLGF binding VEGFR1 increases the VEGF available to bind to VEGFR2, then perhaps some competition will be observed. In this case, high levels of competition (and therefore an impact of PLGF on VEGF activation of VEGFR2) is only seen at low VEGF and high PLGF concentrations (Figs 8A and S28). At high VEGF levels, VEGFR2 is already well activated and thus not responsive to PLGF addition; at low levels of VEGF, only high levels of PLGF will sufficiently saturate VEGFR1 to encourage VEGF transfer to VEGFR2; and even this effect is only seen inside the cell, because at the cell surface the large reservoir again provides too large a buffer. Even the largest such changes are likely too small to observe reliably in an experiment.

Finally, it is known that pH can be different, typically lower, in endosomes than outside the cell and that this can alter the binding rate constants for ligand-receptor binding. We explored whether pH-based differences in ligand-receptor binding would impact some of the key insights here (S29 and S30 Figs). While some small differences in the overall levels of ligand-receptor binding are observed (intracellularly) as a result, the overall system is not greatly changed, for example the decoy effects of VEGFR2 on VEGFR1 and of VEGFR1 and VEGFR2 are essentially unchanged.

Discussion

Proteins must be in the right cellular location at the right time to interact with other proteins and function properly. For transmembrane proteins such as growth factor receptors, endosomal trafficking brings them to the surface and shuttles

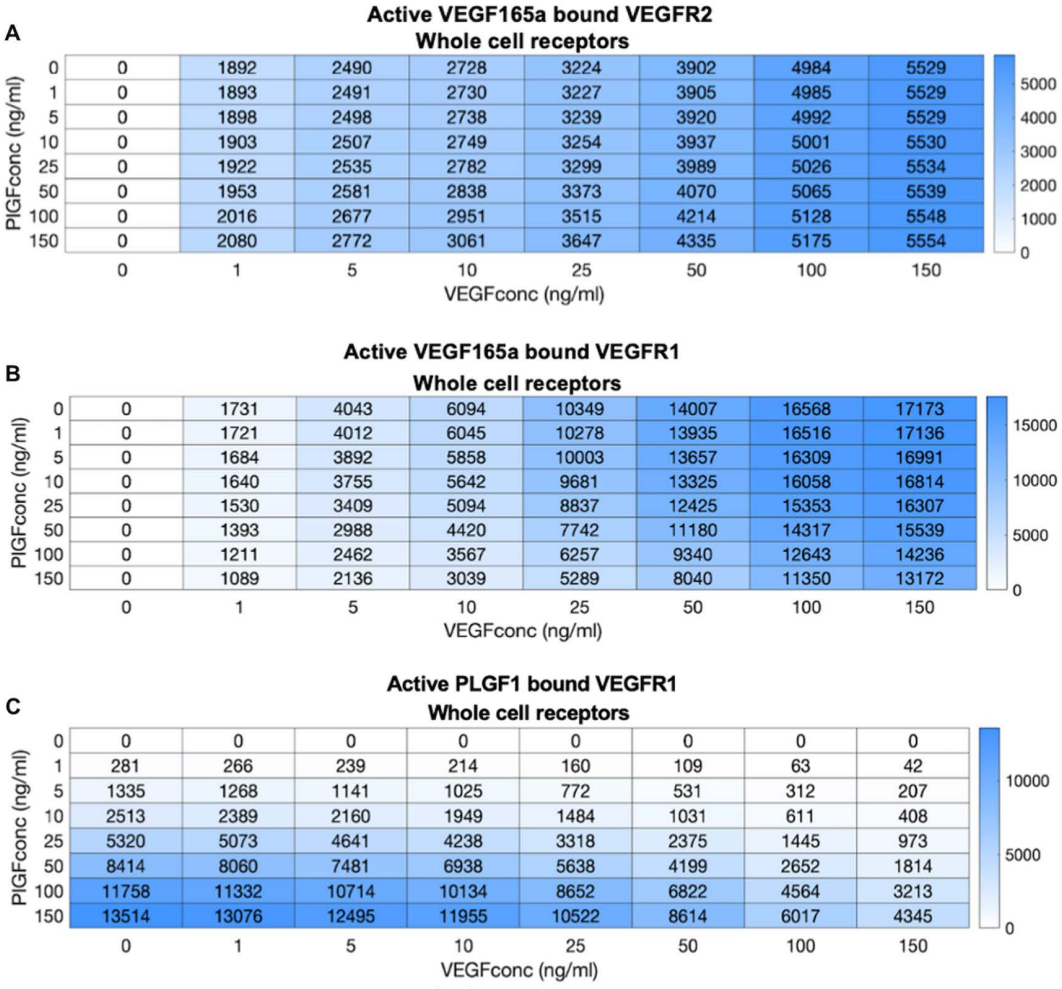

Fig 8. PLGF-VEGF competition: impact on active ligand-bound receptor complexes. Predicted level of active VEGFR.ligand.VEGFR complexes, following two hours of ligand treatment at different doses for $PLGF_1$ and $VEGF_{165a}$, across the whole cell: VEGF-bound VEGFR2 (top), VEGF-bound VEGFR1 (middle), PLGF-bound VEGFR1(bottom).

https://doi.org/10.1371/journal.pcbi.1013254.g008

them between the surface and intracellular locations. These intracellular locations may facilitate receptor degradation, initiation of alternate signaling pathways, or simply be a repository for additional proteins that can come to the surface when required. Whatever their purpose, the localization of the receptors (and therefore their function) is controlled by the processes of intracellular trafficking.

Receptors that bind VEGF family ligands, such as the receptor tyrosine kinases VEGFR1 and VEGFR2, and the co-receptor Neuropilin-1 (NRP1) are no different; to bind to extracellular ligands, they must be on the cell surface. Intracellular-located receptors can only bind a ligand if the ligand is produced cell-autonomously and not secreted; or if extracellular ligand undergoes pinocytosis; or if extracellular ligand is trafficked inwards while bound to receptors.

We recently used a combined computational-experimental approach to quantify the trafficking and localization of VEGFR1, VEGFR2, and NRP1 on human endothelial cells for the first time [41]. In the absence of ligands, we showed that the receptors are constitutively moved around the cell, and that the trafficking rates and thus localization were different for each receptor. For example, VEGFR1 is less stable (has faster turnover) than VEGFR2 or NRP1; and due to

the balance of trafficking processes, VEGFR1 is predominantly located inside the cell, while VEGFR2 is more balanced and NRP1 is more prevalent on the cell-surface. These localization distinctions have implications for ligand interactions, as ligand-receptor binding is considered a primary signal initiation event in many cases. However, we did not know whether ligand binding alters receptor trafficking, beyond previous observations of increased VEGFR2 internalization with ligand binding and receptor activation [35,36,39,54,58,60,61]. Therefore, the aim of this study was to explore trafficking in response to exogenously administered ligands, and to predict how the ligation of cell surface and internal receptors differs.

Using novel experimental data of VEGFR1, VEGFR2, and NRP1 expression, and additional data of VEGFR1, VEGFR2, and NRP1 localization to cell surface or internal cell locations, before and after exposure to two key VEGF family ligands ($VEGF_{165a}$ and the VEGFR1-specific $PLGF_1$), we demonstrated that of the three receptors, only VEGFR2 exhibited significantly different trafficking with ligand engagement. This is the first quantification of ligand-responsive trafficking of VEGFR1 and NRP1, and it is interesting that they did not follow the pattern of higher internalization that VEGFR2 exhibits. In addition, the pattern of the VEGFR2 changes was at first surprising: surface VEGFR2 was decreased as expected, and whole-cell VEGFR2 decreased, but internal VEGFR2 was neither substantially increased in compensation with the surface loss, nor was it decreased reflecting overall receptor loss throughout the cell. Instead, it stayed relatively steady.

Turning to our computational mechanistic model, we used separate observations to parameterize and validate the model, and to explain the mechanistic underpinnings of the observations. We used sensitivity analysis to explore how ligand-induced changes to each of the fifteen trafficking parameters might explain the outcomes. First, the surface loss of VEGFR2 could be parsimoniously explained by a single effect: three-fold increased internalization of ligand-bound VEGFR2 compared to unligated VEGFR2 (Fig 9). Higher internalization of ligand-activated receptor tyrosine kinases has been observed in multiple receptor families, including EGFR [62,63], and is thought to be due to increased association with clathrin pathways [64]. Second, without changing any additional parameters beyond the ligand-induced internalization, the internal and whole-cell levels of VEGFR2 also matched the experimental observations. Along with validating the model, the model showed that the reason the internal receptors did not increase substantially (and only transiently, in the

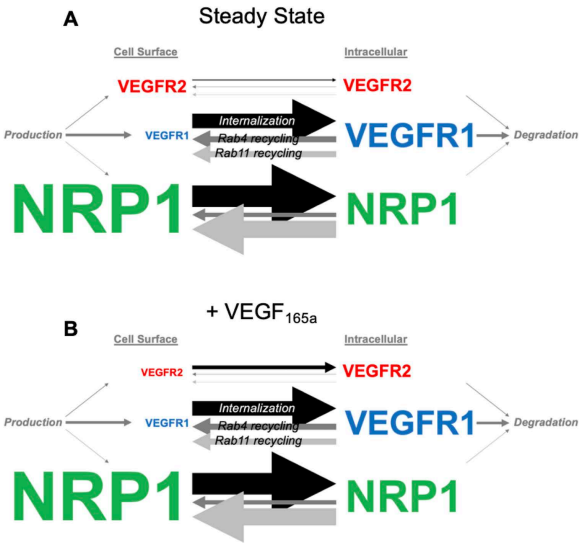

Fig 9. Differences in VEGFR1, VEGFR2 and NRP1 trafficking in the absence of ligands (steady state) and presence of ligands in HUVECs. A, VEGFR1, VEGFR2, NRP1 are constitutively trafficked in the absence of ligands in HUVECs. B, VEGFR2 internalization is faster as a result of $VEGF_{165a}$ treatment. PLGF treatment has no impact on VEGFR1, VEGFR2 or NRP1 trafficking in HUVECs. The size of the arrow represents the amount of receptor movement. The size of the receptor represents the expression level relative to other receptors shown here.

https://doi.org/10.1371/journal.pcbi.1013254.g009

simulations) is that the production of the receptors is balanced by degradation, and thus in the absence of degradation changes the intracellular levels return to their pre-ligand levels quickly. The whole-cell slight decrease is due to a combination of the surface decrease and the steady internal levels. Further validation of the model was obtained by comparing simulations and experiments using siRNA to downregulate the recycling-associated proteins Rab4a and Rab11a. That these knockdowns did not affect VEGF receptor levels was consistent with our previous experimental results in the absence of ligands [41], but knockdown of other trafficking proteins – individually or in combination with knockdown of Rab4a and Rab11a – may provide further insight into the key processes on VEGF receptor trafficking.

As is often the case with models of biological systems, optimized using multimodal data, there remains uncertainty in some of the parameter values of the model. Of the unliganded trafficking parameters, the parameters associated with Neuropilin trafficking were less identifiable and had more uncertainty in the distribution of potential values [41]. Of note, we showed that the behavior of the system overall and the optimization of the other parameters was not substantially affected by this uncertainty. That said, there is potentially further work to be done using uncertainty propagation techniques to explore whether additional experimental data is needed to further constrain the system. Even when some individual parameters are not well constrained, combinations of those parameters can be [65].

Now that we have a handle on receptor trafficking, and how ligand binding affects it, what about the functional reason for studying the system - the formation of signaling-pathway-initiating ligand-receptor complexes? We gained several surprising insights from the simulations. First, active VEGFR2 are predicted to be mostly internal, even though VEGFR2 is evenly distributed between the cell surface and internally before ligand exposure, and even though all ligands in the model were initially extracellular. Second, active VEGFR1 is also mostly internal, which correlates with 90% of VEGFR1 being internal. However, the small VEGFR1 population on the surface was predicted to be sufficient to bring ligands inside the cell. The fast trafficking of VEGFR1 shuttles ligands in; and we know that it's not just ligands internalized via VEGFR2 binding and later released inside the cell, because it works for $PLGF_1$ as well. Third, NRP1 is predicted to exhibit slower trafficking due to its increased association with VEGFR2 (via $VEGF_{165a}$), which has lower trafficking rate constants than VEGFR1 and VEGFR1-NRP1; but NRP1 levels on the surface and inside the cell are not substantially altered.

What is the meaning of predictions that active VEGFR2 and active VEGFR1 are predominantly intracellular? We know that cell signaling pathways are not solely initiated from cell surface receptors. While that has been the typical picture for illustrating ligand-induced receptor signaling, for VEGFR2 and for other receptors we know that (a) intracellular receptors can initiate signaling pathways, and (b) that intracellular receptors can initiate signaling pathways that are different than those initiated by cell surface receptors [53,54,66]. Just as for ligand-receptor binding, context and location are everything. Different subcellular locations host different phosphatases, scaffold proteins, and more to enable differential signaling. Overall observed downstream signaling and cellular behavior is due to a combination of these different signaling pathways following ligand exposure. Second, it is notable that the timing of the signaling can be different - for example, VEGFR2 on the surface has an early activity peak and then declines (due to internalization), while intracellular active VEGFR2 is more sustained [53,54,66]. There are examples of both types of signaling responses in endothelial cells - early peaks or sustained signaling - depending on the signaling pathway and the context. These temporally regulated effects may be linked to the localization of signal initiation, although here we only simulated ligand binding and receptor activation, and did not include additional regulation such as dephosphorylation that might alter these dynamics further. The complex regulation of the downstream pathways themselves, including the known differential localization of site-specific tyrosine phosphatases [53–55,57] may alter both the identity and dynamics of which pathways are activated by the receptor from which locations.

We explored the impact of NRP1 on VEGFR1 and VEGFR2 activation in multiple ways, including simulating a VEGF isoform that does not bind NRP1 ($VEGF_{121a}$) and a PLGF isoform that does ($PLGF_2$). Interestingly, the effects of NRP1 are dose dependent; for example, it is at lower concentrations, which are more typical of *in vivo* conditions than of *in vitro* cell culture, that we see enhanced activation of VEGFR2 activation by $VEGF_{165a}$ vs the non-NRP1 binding $VEGF_{121a}$, and we can also see this effect via a computational knockdown of NRP1 expression. NRP1 also exerts an isoform-specific effect

on VEGFR1 activation, by associating directly with VEGFR1 and facilitating $VEGF_{121a}$ and $PLGF_1$ binding but not that of $VEGF_{165a}$ or $PLGF_2$; this effect is again stronger at lower ligand concentrations typical of *in vivo* conditions.

With a working multi-receptor mechanistic model, we returned to a concept that has been raised before with regard to VEGFR1 and VEGFR2, specifically that VEGFR1, whose kinase and signaling activity is difficult to document in endothelial cells, serves as a 'decoy receptor' for VEGFR2, i.e., that by binding VEGF ligands it takes those ligands away from VEGFR2 and lowers the signaling amplitude of the canonical receptor. There is compelling evidence that this mechanism is operative during development, as VEGFR1 lacking the cytoplasmic domain is sufficient for vascular development while total VEGFR1 deletion leads to embryonic lethality with vascular overgrowth [31,32,67–70]. In adult angiogenesis, VEGFR1 may play a signaling role [30,51,71]. Even while signaling, VEGFR1 may function as a decoy, and thus we developed a metric to quantify this decoy role using computational simulations with and without VEGFR1 present.

Several interesting observations followed. First, in our simulations, VEGFR1 did function as a decoy, reducing the local VEGF available for VEGFR2 to bind and become activated. However, this only occurred intracellularly in our model, where the local VEGF reservoir, even at similar concentration levels, is much smaller than the extracellular reservoir (due to smaller intracellular volumes). We term this the 'reservoir effect'. The decoy effect works by competing for a shared ligand pool; if ligand is not rate-limiting, there is likely no competition. In this model, in intracellular reservoirs the impact on local concentration of one ligand binding/unbinding a receptor is larger due to small volumes. In essence, VEGFR1 can exert a much stronger influence on VEGFR2 inside the cell than outside the cell. The lack of a decoy effect on the cell surface is consistent with previous explorations which did not account for intracellular trafficking [34,44,59], and we also note that *in vivo*, the surface-area-to-volume ratio extracellularly would be much higher than it is *in vitro*, and thus some decoy effect on the surface may occur *in vivo*.

Second, the decoy effect that is observed in the in vitro simulations is much stronger at lower ligand concentrations. This is likely because at high ligand concentrations, the receptors don't have to compete for ligand binding. The effective extracellular ligand concentration is predicted to be lower *in vivo* than concentrations used *in vitro*, and thus we would expect that the decoy effect would be substantial in that situation, possibly even at the cell surface.

There is a second type of decoy effect - rather than receptors competing for ligands, ligands can compete for binding to VEGFR1; in particular, because PLGF1 binds only VEGFR1, it has been proposed to be able to displace other VEGF ligands from VEGFR1 and thus increase binding to VEGFR2. While our simulations show that this effect can occur, unlike receptor competition it is a phenomenon of high ligand levels rather than low ligand levels. Because it is not predicted to occur at lower ligand concentrations, we expect that PLGF-VEGF competition may not be a significant contributor to decoy effects *in vivo*, though in pathological situations ligand and receptor expression may be altered and the effect may come into play.

Here, we did not include autocrine expression of ligands by the endothelial cells themselves, which can occur; for example PLGF and $VEGF_{165a}$ have different expression patterns in vascular endothelial cells [72,73]. The exclusion is justified for *in vitro* cell cultures we are simulating here, as any autocrine expression would be swamped by the high levels of exogenous ligand added. *In vivo*, expression of VEGF ligands by endothelial cells would likely further increase intracellular activation if the ligands encounter receptors before secretion. Another aspect of VEGF biology we have not explored here is the potential for formation of VEGFR1-VEGFR2 heterodimers, which could themselves initiate different signaling pathways than either homodimer. We didn't include it here to avoid further complexity, and because information is not currently available about the relative prevalence of these heterodimers, but also because the two major cellular locations (surface and internal) have two different receptor-expressing regimes: VEGFR2 in excess of VEGFR1 on the surface, VEGFR1 in excess of VEGFR2 intracellularly. This reduces the number of heterodimers that would likely form, though interestingly computational predictions suggest it may also suppress formation of the homodimer of the less abundant receptor [48].

In summary, we have developed and validated a model of multi-VEGF-receptor trafficking under conditions of ligand stimulation in human endothelial cells. A similar approach could be used for other receptor systems and cell types. Many

of the insights developed here for the VEGF-VEGFR system are likely also generalizable to other systems, including: the relative importance of receptor vs ligand competition at low or high ligand concentrations; competition being higher in small-reservoir environments such as intracellular spaces; and the importance of receptor localization on receptor function.

Supporting information

S1 Table. Ligand-receptor interactions. While all four ligands bind VEGFR1, PLGF ligands do not bind VEGFR2. Longer isoforms include a NRP1-binding domain. VEGFR1 and NRP1 can directly interact, and the coupled receptor does not admit the NRP1-binding ligands, rather the non-NRP1-binding ligands can bind to the VEGFR1 in the complex. VEGFR2 and NRP1 do not directly interact, and only form a complex when bridged by a $VEGF_{165a}$ molecule binding to both receptors.
(PDF)

S2 Table. Molecules included in the model. The total number of molecules and molecular complexes in the model is 281. The comprehensive lists of these molecules, and the unique ID number by which each is identified in the code, are given in S3–S11 Tables.
(PDF)

S3 Table. Unligated receptors and receptor complexes. This table gives the unique ID number by which each molecule or molecular complex is identified in the model code. Dots indicate direct binding. These unligated receptors were included in our previous model of the trafficking of only receptors [41].
(PDF)

S4 Table. Unbound ligands. This table gives the unique ID number by which each molecule is identified in the model code. V165 represents $VEGF_{165a}$, V121 represents $VEGF_{121a}$, P1 represents $PLGF_1$, and P2 represents $PLGF_2$.
(PDF)

S5 Table. Ligand-bound monomeric VEGFR1 or VEGFR2. These molecular complexes are non-signaling and primarily are intermediates to ligands binding two receptors. Dots indicate direct binding. This table gives the unique ID number by which each molecule or molecular complex is identified in the model code. V165 represents $VEGF_{165a}$, V121 represents $VEGF_{121a}$, P1 represents $PLGF_1$, and P2 represents $PLGF_2$.
(PDF)

S6 Table. Non-signaling ligand-bound VEGFR1 dimers. Although these complexes include two receptors, they are not coupled by the ligand (i.e., the ligand is bound only to one of the two receptors) and thus are not in higher-propensity signaling conformation. These are also likely to be intermediate forms. Dots and parentheses indicate direct binding; for example, P1.R1(N1).R1 means one $PLGF_1$ is bound to one VEGFR1, and this VEGFR1 is itself bound to another VEGFR1 and to a NRP1. This table gives the unique ID number by which each molecule or molecular complex is identified in the model code. V165 represents $VEGF_{165a}$, V121 represents $VEGF_{121a}$, P1 represents $PLGF_1$, and P2 represents $PLGF_2$.
(PDF)

S7 Table. Non-signaling ligand-bound VEGFR2 dimers. Although these complexes include two receptors, they are not coupled by the ligand (i.e., the ligand is bound only to one of the two receptors) and thus are not in higher-propensity signaling conformation. These are also likely to be intermediate forms. Dots and parentheses indicate direct binding. This table gives the unique ID number by which each molecule or molecular complex is identified in the model code. V165 represents $VEGF_{165a}$ and V121 represents $VEGF_{121a}$.
(PDF)

S8 Table. Nonsignaling NRP1-only complexes. Dots indicate direct binding. This table gives the unique ID number by which each molecule or molecular complex is identified in the model code. V165 represents $VEGF_{165a}$ and P2 represents $PLGF_2$.
(PDF)

S9 Table. Signaling ligand-bound VEGFR1 dimers. This table gives the unique ID number by which each molecule or molecular complex is identified in the model code. Dots indicate direct binding. A Δ symbol indicates that the ligand is bound to both VEGFR1, and that the two VEGFR1 are also directly associated with each other. V165 represents $VEGF_{165a}$, V121 represents $VEGF_{121a}$, P1 represents $PLGF_1$, and P2 represents $PLGF_2$.
(PDF)

S10 Table. Signaling ligand-bound VEGFR2 dimers. This table gives the unique ID number by which each molecule or molecular complex is identified in the model code. Dots and parentheses indicate direct binding. A Δ symbol indicates that the ligand is bound to both VEGFR2, and that the two VEGFR2 are also directly associated with each other. V165 represents $VEGF_{165a}$ and V121 represents $VEGF_{121a}$.
(PDF)

S11 Table. Matrix-bound complexes. Due to the size of matrix molecules, these complexes are only at the surface and are not internalized. However, ligand-coupled receptors can still serve as signal initiation [53]. This table gives the unique ID number by which each molecule or molecular complex is identified in the model code. Dots and parentheses indicate direct binding. A Δ symbol indicates that the ligand is bound to both VEGFR, and that the two VEGFR are also associated. This table is included for complete description of the code provided, however in the present study matrix binding is not included and all these molecules will have zero concentration. V165 represents $VEGF_{165a}$, V121 represents $VEGF_{121a}$, P1 represents $PLGF_1$, and P2 represents $PLGF_2$.
(PDF)

S12 Table. Model Parameters. Compartment volumes, compartment surface areas, and initial concentrations of ligands and surface receptors. Ligand molecular weights were obtained from sources of experimental recombinant proteins. Includes sources for justification of key parameters from previous studies [41,74,75].
(PDF)

S13 Table. Production rates for VEGF receptors. These parameters are obtained from optimization in the absence of ligands, and result in steady state surface receptor densities in agreement with previous measurements [41], when used in concert with the trafficking parameters in S14 Table.
(PDF)

S14 Table. Trafficking parameter estimates for VEGFR1, VEGFR2, and NRP1 in the absence and presence of ligands based on experimental data from HUVEC. This standard parameter set was used for model simulations presented in the main manuscript. Based on modeling and data from HUVECs (Human Umbilical Vein Endothelial Cells). Unligated VEGFR1, VEGFR2, and NRP1 trafficking parameters are from previous work [41]; ligated trafficking parameters are described in this study. R1: VEGFR1, R2: VEGFR2, N1: Neuropilin-1 or NRP1.
(PDF)

S15 Table. Receptor dimerization parameters. R1: VEGFR1, R2: VEGFR2, N1: Neuropilin-1/NRP1. The unligated receptor dimerization rates were set in a previous study to yield 30–40% dimers of R1-R1, R2-R2, and N1-R1 [41]. Note that these base parameters (in units of $molecules^{-1}.\mu m^2.s^{-1}$) are adjusted to units of $molecules^{-1}.cell.s^{-1}$ at each location, using the appropriate membrane surface area (S12 Table), as described previously [41]. Includes sources for justification of key parameters from previous studies [7,8,41,45,53,76].
(PDF)

S16 Table. Experimentally-derived 1:1 Ligand-Receptor binding. Measured and estimated rate constants and equilibrium constants assuming 1:1 interaction (i.e., monovalent ligand binds monovalent receptor dimer fully in one step; this is the most common assumption for estimating ligand-receptor binding experimentally). These are not the values used in our model, which is a dimerization-explicit model, but the parameters used (S17 Table) are based on these as described in the Methods section. In each entry the units of the parameters shown are (top to bottom): K_D (pM), k_{on} (pM^{-1} s^{-1}), and k_{off} (s^{-1}). L: Ligand; R1: VEGFR1; R2: VEGFR2; N1: NRP1. Includes sources for justification of key parameters from previous studies [34,53,76–79].
(PDF)

S17 Table. Ligand-Receptor binding. Calculated rate constants for first binding step to monomers or dimers assuming 1:2 interaction (i.e., one bivalent ligand can bind to two monovalent receptor monomers, or twice to one bivalent receptor dimer). The base on-rate constants (k_{on}) are assumed to be one quarter of the 1:1 rate constant (S16 Table) to account for the bivalency of ligands and of receptor dimers. Thus, when considering these base on-rate constant values below, ligand binding to a receptor monomer is twice the rate constant (due to two receptor-binding sites on the ligand) and ligand binding to an unliganded receptor dimer is four times the rate constant (due to two receptor-binding sites on the ligands and two ligand-binding sites on the receptor dimer). L: Ligand; R1: VEGFR1; R2: VEGFR2; N1: NRP1.
(PDF)

S18 Table. Ligand-Receptor Coupling. These are the values for intermolecular and intramolecular binding of ligands and receptors following the first ligand-receptor binding event. Values for receptor-receptor coupling without a ligand ($k_{on,RR}$) are given in S15 Table. The binding rate constant for a ligand (already bound to a receptor monomer) binding to a second receptor monomer ($k_{on,LR}$); the binding rate constant for a ligand (already bound to one receptor in a dimer) binding to the second receptor in a dimer ($k_{\Delta,LR}$); and the binding rate constant for a receptor binding to the second receptor of a dimer (when both are already bound to a ligand) ($k_{\Delta,RR}$) are calculated based on other known parameters as described in *Methods* and in a previous publication [48]. L: Ligand; R1: VEGFR1; R2: VEGFR2; N1: NRP1.
(PDF)

S19 Table. List of experimental reagents and antibodies.
(PDF)

S1 Text. Reconstructing equations from the provided tables and the model code.
(PDF)

S1 Fig. Simulated Scatchard plots comparing different representations of VEGFR dimerization. The system was simulated under three different assumptions: one-to-one ("121") ligand receptor binding, i.e., pre-dimerization of receptors and single step ligand binding/activation; ligand-induced dimerization ("LID"), i.e., no receptor pre-dimerization; and a full dimerization model including all dimerization paths ("All"). The similarity between the "121" and "All" lines indicates that the dimerization model represents the observed equilibrium data well. Top row: VEGFR1 expression only; bottom row: VEGFR2 expression only.
(PDF)

S2 Fig. Distribution of VEGFR2 over 4 hours of $VEGF_{165a}$ treatment. Total (ligated and unligated) receptor levels on the cell surface, inside the cell, and across the whole cell in response to $VEGF_{165a}$ treatment at different levels of how the ligand binding affects the indicated VEGFR2 trafficking parameter. Simulations are shown as solid and dotted lines. Gray arrows indicate the direction of increasing parameter values. The same experimental data is shown in each row as dots and variance bars. A-C, $VEGF_{165a}$ binding causes an increase in the internalization rate constant for VEGFR2 (V.R2.kint and V.R2.N1.kint), compared to the unligated value; a three-fold increase (solid line) compared to the unligated receptor rate constant matched the observed data best. D-O, Taking this increased k_{int} (receptor complex internalization rate) as

a baseline for the remaining simulations, we explored variation in the other trafficking parameters. Lines represent 5x, 2x, 1x, 0.5x, 0.2x the baseline (unligated) trafficking rate; in panels D and G-O the lines overlap substantially. D-F, total surface, internal and whole cell receptors in response to $VEGF_{165a}$ treatment and change in ligated VEGFR2 degradation (altered k_{deg} affecting both V.R2 and V.R2.N1 complexes). G-O, total surface, internal and whole cell receptors in response to $VEGF_{165a}$ treatment and change in ligated VEGFR2 recycling, including: recycling via Rab4a (altered k_{rec4}, G-I); transfer to Rab11a (altered k_{4to11}, J-L); and recycling via Rab11a (altered k_{rec11}, M-O). Altered rate constants affect both V.R2 and V.R2.N1 complexes. Panels A-F are identical to panels A-F of Fig 3; they are replicated here for ease of comparison. Gray arrows indicate the direction of increasing parameter values.
(PDF)

S3 Fig. Distribution of VEGFR1 over 4 hours of $VEGF_{165a}$ treatment. Total (ligated and unligated) receptor levels on the cell surface, inside the cell, and across the whole cell in response to $VEGF_{165a}$ treatment at different levels of how the ligand binding affects the indicated VEGFR1 trafficking parameter. Simulations are shown as solid and dotted lines. Lines represent 5x, 2x, 1x, 0.5x, 0.2x the baseline (unligated) trafficking rate. Gray arrows indicate the direction of increasing parameter values. The same experimental data is shown in each row as dots and variance bars. A-C, Response to $VEGF_{165a}$ treatment for different values of the ligated VEGFR1 internalization parameter (k_{int}. D-F, Response to $VEGF_{165a}$ treatment for different values of the ligated VEGFR1 degradation parameter (k_{deg}), G-I, Tesponse to $VEGF_{165a}$ treatment for different values of the ligated VEGFR1 fast recycling via Rab4a-expressing endosomes parameter (k_{rec4}), J-L, Response to $VEGF_{165a}$ treatment for different ligated VEGFR1 transfer from Rab4a-expressing endosomes to Rab11a-expressing endosomes parameter (k_{4to11}), M-O, Response to $VEGF_{165a}$ treatment for different values of the ligated VEGFR1 slow recycling via Rab11a-expressing endosomes parameter (k_{rec11}).
(PDF)

S4 Fig. Distribution of VEGFR1 over 4 hours of $PLGF_1$ treatment. Total (ligated and unligated) receptor levels on the cell surface, inside the cell, and across the whole cell in response to $PLGF_1$ treatment at different levels of how the ligand binding affects the indicated VEGFR1 trafficking parameter. Simulations are shown as solid and dotted lines. Lines represent 5x, 2x, 1x, 0.5x, 0.2x the baseline (unligated) trafficking rate. Gray arrows indicate the direction of increasing parameter values. The same experimental data is shown in each row as dots and variance bars. A-C, Response to PLGF1 treatment for different values of the ligated VEGFR1 internalization parameter (k_{int}, applies to both P.R1 and P.R1.N1 complexes), D-F, Response to $PLGF_1$ treatment for different values of the ligated VEGFR1 degradation parameter (k_{deg}), G-I, Response to $PLGF_1$ treatment for different values of the ligated VEGFR1 fast recycling via Rab4a-expressing endosomes parameter (k_{rec4}), J-L, Response to $PLGF_1$ treatment for different values of the ligated VEGFR1 transfer from Rab4a-expressing endosomes to Rab11a-expressing endosomes parameter (k_{4to11}), M-O, Response to $PLGF_1$ treatment for different values of the ligated VEGFR1 slow recycling via Rab11a-expressing endosomes parameter (k_{rec11}).
(PDF)

S5 Fig. Summary of impact of trafficking parameters on localization of VEGF receptors following VEGF ligation. Predicted levels of VEGFR1, VEGFR2, and NRP1 at the surface, internally, and across the whole cell ("total") after 0, 60, or 240 mins treatment with 50 $ng.mL^{-1}$ of $VEGF_{165a}$ (A-B), or $VEGF_{121a}$ (C-D). Each row represents simulations with a different ligated receptor trafficking parameter increased five-fold. Changes in receptor levels normalized to the no-ligand condition (0 mins) are shown (A,C). These are further normalized to the no-parameter-change ("ctrl") condition (B,D), demonstrating the small number of parameters that alter receptor localization.
(PDF)

S6 Fig. Summary of impact of trafficking parameters on localization of VEGF receptors following PLGF ligation. Predicted levels of VEGFR1, VEGFR2, and NRP1 at the surface, internally, and across the whole cell ("total") after 0, 60, or 240 mins treatment with 50 $ng.mL^{-1}$ of $PLGF_1$ (A-B) or $PLGF_2$ (C-D). Each row represents simulations with a different

ligated receptor trafficking parameter increased five-fold. Changes in receptor levels normalized to the no-ligand condition (0 mins) are shown (A,C). These are further normalized to the no-parameter-change ("ctrl") condition (B,D), demonstrating the small number of parameters that alter receptor localization.
(PDF)

S7 Fig. Differential receptor fluxes. The overall transport rates (rate constant multiplied by concentration) for VEGFR1, VEGFR2, and NRP1 in each subcellular location at steady state (no ligand treatment) and under different durations of ligand treatment. A rate constant may be high, but if the corresponding concentration is low (and we know that the receptors are not uniformly distributed across cellular compartments), then the rate of movement will be low. Note also that the x-axis scale is different for each receptor. At steady state, these overall rates in and out are balanced, so the 'net' rates are close to zero. For Rab11a: receptors arriving from Rab4a are balanced out by recycling; for Rab4a: receptors internalized to Rab4a are balanced out the sum of degraded and recycling; for surface: receptor internalization balances the sum of new synthesis and recycling. "degr." = degradation; "prodn." = production. A-C, transport rates for VEGFR1, VEGFR2, and NRP1 at steady state starvation conditions (no ligand treatment), D-F, transport rates for VEGFR1, VEGFR2, and NRP1 after 1 hour of 50 ng.mL^{-1} $VEGF_{165a}$ treatment, G-I, transport rates for VEGFR1, VEGFR2, and NRP1 after 4 hours of 50 ng.mL^{-1} $VEGF_{165a}$ treatment.
(PDF)

S8 Fig. Surface, internal and whole cell levels of total (unligated and ligated) VEGFR1, VEGFR2, and NRP1 after Rab4a/Rab11a knockdown, compared to control (no siRNA treatment) under A-C, 1 hour of HUVEC treatment with 50 ng.mL^{-1} of $VEGF_{165a}$. D-F, 4 hours of HUVEC treatment with 50 ng.mL^{-1} of $VEGF_{165a}$. G-I, 1 hour of HUVEC treatment with 50 ng.mL^{-1} of $PLGF_{1}$. J-L, 4 hours of HUVEC treatment with 50 ng.mL^{-1} of $PLGF_{1}$.
(PDF)

S9 Fig. Active VEGFR2 following VEGF treatment. Previous supplemental figures S2–S7 Figs have illustrated localization of all receptors, without regard to whether they are in complexes with other receptors or ligands. Here, we focus on active, ligated receptors. Number of active (ligand-dimerized) VEGFR2 receptors on the whole cell (A-C), cell surface (D-F), and internally (G-I) following 15 min, 60 min, or 240 min of treatment with $VEGF_{121a}$ or $VEGF_{165a}$.
(PDF)

S10 Fig. Active VEGFR1 following VEGF or PLGF treatment. Number of active (ligand-dimerized) VEGFR1 receptors on the whole cell (A-C), cell surface (D-F), and internally (G-I) following 15 min, 60 min, or 240 min of treatment with $VEGF_{121a}$, $VEGF_{165a}$, $PLGF_{1}$, or $PLGF_{2}$.
(PDF)

S11 Fig. Ligand dose-dependent distribution of ligated VEGFR2. different single ligand doses 2.5, 25, 50, 100, 200 ng.mL^{-1} of A-C, $VEGF_{121a}$ treatment or D-F, $VEGF_{165a}$ treatment.
(PDF)

S12 Fig. Ligand dose-dependent distribution of ligated VEGFR1. different single ligand doses 2.5, 25, 50, 100, 200 ng.mL^{-1} of A-C, $VEGF_{121a}$, D-F, $VEGF_{165a}$, G-I, $PLGF_{1}$ or J-L, $PLGF_{2}$.
(PDF)

S13 Fig. Dimerization of VEGFR1, VEGFR2 and NRP1. VEGF receptors can be dimerized in the absence of ligand; they can also be ligand-bound and dimerized without being active (if the ligand is not bound to both receptors). These graphs show the impact on receptor dimerization (not activation) across the whole cell (A-C), or on the cell surface (D-F) after 240 min of treatment with 50 ng.ml^{-1} $VEGF_{121a}$, $VEGF_{165a}$, $PLGF_{1}$, or $PLGF_{2}$.
(PDF)

S14 Fig. Fraction of VEGFR1-NRP1 heterodimers. VEGFR1 and NRP1 can associate without ligands [45], and the VEGFR1-NRP1 complex formation affected by the presence of ligands that can bind to the complex ($VEGF_{121a}$ and $PLGF_1$) and those that cannot ($VEGF_{165a}$ and $PLGF_2$). These graphs show the impact of VEGFR1-NRP1 dimerization across the whole cell (A-B) or on the cell surface (C-D) after 240 minutes of 50 $ng.ml^{-1}$ $VEGF_{121a}$, $VEGF_{165a}$, $PLGF_1$, or $PLGF_2$.
(PDF)

S15 Fig. Impact of NRP1 expression on whole cell VEGFR2 activation by $VEGF_{165a}$. A, VEGFR2.$VEGF_{165a}$.VEGFR2 levels for different initial $VEGF_{165a}$ concentrations. B, VEGFR2.$VEGF_{165a}$.VEGFR2 levels in the absence of NRP1 for different initial $VEGF_{165a}$ concentrations. C, percent change in VEGFR2.$VEGF_{165a}$.VEGFR2 levels due to loss of NRP1 for different initial $VEGF_{165a}$ concentrations.
(PDF)

S16 Fig. Impact of NRP1 expression on surface VEGFR2 activation by $VEGF_{165a}$. A, VEGFR2.$VEGF_{165a}$.VEGFR2 levels for different initial $VEGF_{165a}$ concentrations. B, VEGFR2.$VEGF_{165a}$.VEGFR2 levels in the absence of NRP1 for different initial $VEGF_{165a}$ concentrations. C, percent change in VEGFR2.$VEGF_{165a}$.VEGFR2 levels due to loss of NRP1 for different initial $VEGF_{165a}$ concentrations.
(PDF)

S17 Fig. Impact of NRP1 expression on internal VEGFR2 activation by $VEGF_{165a}$. A, VEGFR2.$VEGF_{165a}$.VEGFR2 levels for different initial $VEGF_{165a}$ concentrations. B, VEGFR2.$VEGF_{165a}$.VEGFR2 levels in the absence of NRP1 for different initial $VEGF_{165a}$ concentrations. C, percent change in VEGFR2.$VEGF_{165a}$.VEGFR2 levels due to loss of NRP1 for different initial $VEGF_{165a}$ concentrations.
(PDF)

S18 Fig. Impact of NRP1 expression on whole cell VEGFR1 activation by $VEGF_{165a}$. A, VEGFR1.$VEGF_{165a}$.VEGFR1 levels for different initial $VEGF_{165a}$ concentrations. B, VEGFR1.$VEGF_{165a}$.VEGFR1 levels in the absence of NRP1 for different initial $VEGF_{165a}$ concentrations. C, percent change in VEGFR1.$VEGF_{165a}$.VEGFR1 levels due to loss of NRP1 for different initial $VEGF_{165a}$ concentrations.
(PDF)

S19 Fig. Impact of NRP1 expression on surface VEGFR1 activation by $VEGF_{165a}$. A, VEGFR1.$VEGF_{165a}$.VEGFR1 levels for different initial $VEGF_{165a}$ concentrations. B, VEGFR1.$VEGF_{165a}$.VEGFR1 levels in the absence of NRP1 for different initial $VEGF_{165a}$ concentrations C, percent change in VEGFR1.$VEGF_{165a}$.VEGFR1 levels due to loss of NRP1 for different initial $VEGF_{165a}$ concentrations.
(PDF)

S20 Fig. Impact of NRP1 expression on internal VEGFR1 activation by $VEGF_{165a}$. A, VEGFR1.$VEGF_{165a}$.VEGFR1 levels for different initial $VEGF_{165a}$ concentrations. B, VEGFR1.$VEGF_{165a}$.VEGFR1 levels in the absence of NRP1 for different initial $VEGF_{165a}$ concentrations. C, percent change in VEGFR1.$VEGF_{165a}$.VEGFR1 levels due to loss of NRP1 for different initial $VEGF_{165a}$ concentrations.
(PDF)

S21 Fig. Impact of VEGFR2 expression on whole cell VEGFR1 activation by $VEGF_{165a}$. A, VEGFR1.$VEGF_{165a}$.VEGFR1 levels for different initial $VEGF_{165a}$ concentrations. B, VEGFR1.$VEGF_{165a}$.VEGFR1 levels in the absence of VEGFR2 for different initial $VEGF_{165a}$ concentrations. C, percent change in VEGFR1.$VEGF_{165a}$.VEGFR1 levels due to loss of VEGFR2 for different initial $VEGF_{165a}$ concentrations.
(PDF)

S22 Fig. Impact of VEGFR2 expression on surface VEGFR1 activation by $VEGF_{165a}$. A, VEGFR1.$VEGF_{165a}$.VEGFR1 levels for different initial $VEGF_{165a}$ concentrations. B, VEGFR1.$VEGF_{165a}$.VEGFR1 levels in the absence of VEGFR2 for different initial $VEGF_{165a}$ concentrations. C, percent change in VEGFR1.$VEGF_{165a}$.VEGFR1 levels due to VEGFR2 for different initial $VEGF_{165a}$ concentrations.
(PDF)

S23 Fig. Impact of VEGFR2 expression on internal VEGFR1 activation by $VEGF_{165a}$. A, VEGFR1.$VEGF_{165a}$.VEGFR1 levels for different initial $VEGF_{165a}$ concentrations. B, VEGFR1.$VEGF_{165a}$.VEGFR1 levels in the absence of VEGFR2 for different initial $VEGF_{165a}$ concentrations. C, percent change in VEGFR1.$VEGF_{165a}$.VEGFR1 levels due to VEGFR2 for different initial $VEGF_{165a}$ concentrations.
(PDF)

S24 Fig. Induction of active VEGFR1 by $PLGF_1$. A, Surface, B, Internal, and C, Whole cell levels of VEGFR1.PLGF1.VEGFR1 complexes at different timepoints over 4 hours and under varying PLGF1 concentration.
(PDF)

S25 Fig. PLGF-VEGF competition: impact on active VEGF-bound VEGFR1 complexes. Predicted level of active VEGFR1.VEGF.VEGFR1 complexes, following two hours of ligand treatment at different doses for $PLGF_1$ and $VEGF_{165}$, across the whole cell (top), on the cell surface (middle), and intracellularly (bottom).
(PDF)

S26 Fig. PLGF-VEGF competition: impact on active PLGF-bound VEGFR1 complexes. Predicted level of active VEGFR1.PLGF.VEGFR1 complexes, following two hours of ligand treatment at different doses for $PLGF_1$ and $VEGF_{165}$, across the whole cell (top), on the cell surface (middle), and intracellularly (bottom).
(PDF)

S27 Fig. PLGF-VEGF competition: ligand levels. Predicted level of free (unbound) $VEGF_{165}$ (top) or $PLGF_1$ (bottom), at the cell surface or intracellularly, following two hours of ligand treatment at different doses for $PLGF_1$ and $VEGF_{165}$. Ligand levels are given in units of #/cell.
(PDF)

S28 Fig. PLGF-VEGF competition: impact on active VEGF-bound VEGFR2 complexes. Predicted level of active VEGFR2.VEGF.VEGFR2 complexes, following two hours of ligand treatment at different doses for $PLGF_1$ and $VEGF_{165}$, across the whole cell (top), on the cell surface (middle), and intracellularly (bottom).
(PDF)

S29 Fig. Effect of change in endosomal pH on VEGFR2 activation and decoy effect. Simulations with slower (top) or faster (bottom) rate constants in the endosomes than on the cell surface, due to pH differences. Effect of 4 hours of 50 $ng.mL^{-1}$ $VEGF_{165a}$ treatment on the intracellular levels of VEGFR2.$VEGF_{165a}$.VEGFR2 in HUVECs.
(PDF)

S30 Fig. Effect of change in endosomal pH on VEGFR1 activation and decoy effect. Simulations with slower (top) or faster (bottom) rate constants in the endosomes than on the cell surface, due to pH differences. Effect of 4 hours of 50 $ng.mL^{-1}$ $VEGF_{165a}$ treatment on the intracellular levels of VEGFR1.$VEGF_{165a}$.VEGFR1 in HUVECs.
(PDF)

Author contributions

Conceptualization: Sarvenaz Sarabipour, Karina Kinghorn, Kaitlyn M Quigley, Anita Kovacs-Kasa, Brian H Annex, Victoria L Bautch, Feilim Mac Gabhann.

Data curation: Sarvenaz Sarabipour, Karina Kinghorn, Kaitlyn M Quigley, Anita Kovacs-Kasa, Brian H Annex, Victoria L Bautch, Feilim Mac Gabhann.

Formal analysis: Sarvenaz Sarabipour, Karina Kinghorn, Kaitlyn M Quigley, Anita Kovacs-Kasa, Brian H Annex, Victoria L Bautch, Feilim Mac Gabhann.

Funding acquisition: Brian H Annex, Victoria L Bautch, Feilim Mac Gabhann.

Investigation: Sarvenaz Sarabipour, Karina Kinghorn, Kaitlyn M Quigley, Anita Kovacs-Kasa, Brian H Annex, Victoria L Bautch, Feilim Mac Gabhann.

Methodology: Sarvenaz Sarabipour, Karina Kinghorn, Kaitlyn M Quigley, Anita Kovacs-Kasa, Brian H Annex, Victoria L Bautch, Feilim Mac Gabhann.

Project administration: Brian H Annex, Victoria L Bautch, Feilim Mac Gabhann.

Resources: Brian H Annex, Victoria L Bautch, Feilim Mac Gabhann.

Software: Sarvenaz Sarabipour, Feilim Mac Gabhann.

Supervision: Brian H Annex, Victoria L Bautch, Feilim Mac Gabhann.

Validation: Sarvenaz Sarabipour, Karina Kinghorn, Kaitlyn M Quigley, Anita Kovacs-Kasa, Brian H Annex, Victoria L Bautch, Feilim Mac Gabhann.

Visualization: Sarvenaz Sarabipour, Karina Kinghorn, Kaitlyn M Quigley, Feilim Mac Gabhann.

Writing – original draft: Sarvenaz Sarabipour, Karina Kinghorn, Kaitlyn M Quigley, Anita Kovacs-Kasa, Brian H Annex, Victoria L Bautch, Feilim Mac Gabhann.

Writing – review & editing: Sarvenaz Sarabipour, Karina Kinghorn, Kaitlyn M Quigley, Anita Kovacs-Kasa, Brian H Annex, Victoria L Bautch, Feilim Mac Gabhann.

References

1. Bautch VL. VEGF-directed blood vessel patterning: from cells to organism. Cold Spring Harb Perspect Med. 2012;2(9):a006452. https://doi.org/10.1101/cshperspect.a006452 PMID: 22951440
2. Carmeliet P. Mechanisms of angiogenesis and arteriogenesis. Nat Med. 2000;6(4):389–95. https://doi.org/10.1038/74651 PMID: 10742145
3. Jeltsch M, Leppänen VM, Saharinen P, Alitalo K. Receptor tyrosine kinase-mediated angiogenesis. Cold Spring Harb Perspect Biol. 2013;5(9):a009183.
4. Annex BH. Therapeutic angiogenesis for critical limb ischaemia. Nat Rev Cardiol. 2013;10(7):387–96. https://doi.org/10.1038/nrcardio.2013.70 PMID: 23670612
5. Annex BH, Cooke JP. New Directions in Therapeutic Angiogenesis and Arteriogenesis in Peripheral Arterial Disease. Circ Res. 2021;128(12):1944–57. https://doi.org/10.1161/CIRCRESAHA.121.318266 PMID: 34110899
6. Clegg LE, Ganta VC, Annex BH, Mac Gabhann F. Systems Pharmacology of VEGF165b in Peripheral Artery Disease. CPT Pharmacomet Syst Pharmacol 2017;6(12): 833–44.
7. Sarabipour S, Ballmer-Hofer K, Hristova K. VEGFR-2 conformational switch in response to ligand binding. Elife. 2016;5:e13876. https://doi.org/10.7554/eLife.13876 PMID: 27052508
8. da Rocha-Azevedo B, Lee S, Dasgupta A, Vega AR, de Oliveira LR, Kim T, et al. Heterogeneity in VEGF Receptor-2 Mobility and Organization on the Endothelial Cell Surface Leads to Diverse Models of Activation by VEGF. Cell Rep. 2020;32(13):108187. https://doi.org/10.1016/j.celrep.2020.108187 PMID: 32997988
9. Prahst C, Héroult M, Lanahan AA, Uziel N, Kessler O, Shraga-Heled N, et al. Neuropilin-1-VEGFR-2 complexing requires the PDZ-binding domain of neuropilin-1. J Biol Chem. 2008;283(37):25110–4.
10. Simons M, Gordon E, Claesson-Welsh L. Mechanisms and regulation of endothelial VEGF receptor signalling. Nat Rev Mol Cell Biol. 2016;17(10):611–25. https://doi.org/10.1038/nrm.2016.87 PMID: 27461391
11. Lee H-W, Shin JH, Simons M. Flow goes forward and cells step backward: endothelial migration. Exp Mol Med. 2022;54(6):711–9. https://doi.org/10.1038/s12276-022-00785-1 PMID: 35701563
12. Dewerchin M, Carmeliet P. PlGF: a multitasking cytokine with disease-restricted activity. Cold Spring Harb Perspect Med. 2012;2(8):a011056. https://doi.org/10.1101/cshperspect.a011056 PMID: 22908198

13. Markovic-Mueller S, Stuttfeld E, Asthana M, Weinert T, Bliven S, Goldie KN, et al. Structure of the Full-length VEGFR-1 Extracellular Domain in Complex with VEGF-A. Structure. 2017;25(2):341–52. https://doi.org/10.1016/j.str.2016.12.012 PMID: 28111021
14. Ballmer-Hofer K, Andersson AE, Ratcliffe LE, Berger P. Neuropilin-1 promotes VEGFR-2 trafficking through Rab11 vesicles thereby specifying signal output. Blood. 2011;118(3):816–26. https://doi.org/10.1182/blood-2011-01-328773 PMID: 21586748
15. Nowak DG, Woolard J, Amin EM, Konopatskaya O, Saleem MA, Churchill AJ, et al. Expression of pro- and anti-angiogenic isoforms of VEGF is differentially regulated by splicing and growth factors. J Cell Sci. 2008;121(Pt 20):3487–95. https://doi.org/10.1242/jcs.016410 PMID: 18843117
16. Rivron NC, Vrij EJ, Rouwkema J, Le Gac S, van den Berg A, Truckenmüller RK, et al. Tissue deformation spatially modulates VEGF signaling and angiogenesis. Proc Natl Acad Sci U S A. 2012;109(18):6886–91. https://doi.org/10.1073/pnas.1201626109 PMID: 22511716
17. Ruhrberg C, Gerhardt H, Golding M, Watson R, Ioannidou S, Fujisawa H, et al. Spatially restricted patterning cues provided by heparin-binding VEGF-A control blood vessel branching morphogenesis. Genes Dev. 2002;16(20):2684–98.
18. Yonekura H, Sakurai S, Liu X, Migita H, Wang H, Yamagishi S, et al. Placenta growth factor and vascular endothelial growth factor B and C expression in microvascular endothelial cells and pericytes. Implication in autocrine and paracrine regulation of angiogenesis. J Biol Chem. 1999;274(49):35172–8. https://doi.org/10.1074/jbc.274.49.35172 PMID: 10575000
19. Persico MG, Vincenti V, DiPalma T. Structure, expression and receptor-binding properties of placenta growth factor (PlGF). Curr Top Microbiol Immunol. 1999;237:31–40. https://doi.org/10.1007/978-3-642-59953-8_2 PMID: 9893344
20. Vempati P, Popel AS, Mac Gabhann F. Extracellular regulation of VEGF: isoforms, proteolysis, and vascular patterning. Cytokine Growth Factor Rev. 2014;25(1):1–19. https://doi.org/10.1016/j.cytogfr.2013.11.002 PMID: 24332926
21. Ng YS, Rohan R, Sunday ME, Demello DE, D'Amore PA. Differential expression of VEGF isoforms in mouse during development and in the adult. Dev Dyn. 2001;220(2):112–21. https://doi.org/10.1002/1097-0177(2000)9999:9999<::AID-DVDY1093>3.0.CO;2-D PMID: 11169844
22. Grunstein J, Masbad JJ, Hickey R, Giordano F, Johnson RS. Isoforms of vascular endothelial growth factor act in a coordinate fashion to recruit and expand tumor vasculature. Mol Cell Biol. 2000;20(19):7282–91.
23. Lee S, Jilani SM, Nikolova GV, Carpizo D, Iruela-Arispe ML. Processing of VEGF-A by matrix metalloproteinases regulates bioavailability and vascular patterning in tumors. J Cell Biol. 2005;169(4):681–91. https://doi.org/10.1083/jcb.200409115 PMID: 15911882
24. Selvaraj SK, Giri RK, Perelman N, Johnson C, Malik P, Kalra VK. Mechanism of monocyte activation and expression of proinflammatory cytochemokines by placenta growth factor. Blood. 2003;102(4):1515–24. https://doi.org/10.1182/blood-2002-11-3423 PMID: 12689930
25. Yang X, Zhang Y, Yang Y, Lim S, Cao Z, Rak J, et al. Vascular endothelial growth factor-dependent spatiotemporal dual roles of placental growth factor in modulation of angiogenesis and tumor growth. Proc Natl Acad Sci U S A. 2013;110(34):13932–7. https://doi.org/10.1073/pnas.1309629110 PMID: 23918367
26. Carmeliet P, Moons L, Luttun A, Vincenti V, Compernolle V, De Mol M, et al. Synergism between vascular endothelial growth factor and placental growth factor contributes to angiogenesis and plasma extravasation in pathological conditions. Nat Med. 2001;7(5):575–83.
27. Gigante B, Tarsitano M, Cimini V, De Falco S, Persico MG. Placenta growth factor is not required for exercise-induced angiogenesis. Angiogenesis. 2004;7(3):277–84.
28. Bais C, Wu X, Yao J, Yang S, Crawford Y, McCutcheon K, et al. PlGF Blockade Does Not Inhibit Angiogenesis during Primary Tumor Growth. Cell. 2010;141(1):166–77.
29. Xiang L, Varshney R, Rashdan NA, Shaw JH, Lloyd PG. Placenta growth factor and vascular endothelial growth factor a have differential, cell-type specific patterns of expression in vascular cells. Microcirculation. 2014;21(5):368–79. https://doi.org/10.1111/micc.12113 PMID: 24410720
30. Nesmith JE, Chappell JC, Cluceru JG, Bautch VL. Blood vessel anastomosis is spatially regulated by Flt1 during angiogenesis. Development. 2017;144(5):889–96. https://doi.org/10.1242/dev.145672 PMID: 28246215
31. Kappas NC, Zeng G, Chappell JC, Kearney JB, Hazarika S, Kallianos KG, et al. The VEGF receptor Flt-1 spatially modulates Flk-1 signaling and blood vessel branching. J Cell Biol. 2008;181(5):847–58. https://doi.org/10.1083/jcb.200709114 PMID: 18504303
32. Hiratsuka S, Minowa O, Kuno J, Noda T, Shibuya M. Flt-1 lacking the tyrosine kinase domain is sufficient for normal development and angiogenesis in mice. Proc Natl Acad Sci U S A. 1998;95(16):9349–54. https://doi.org/10.1073/pnas.95.16.9349 PMID: 9689083
33. Autiero M, Waltenberger J, Communi D, Kranz A, Moons L, Lambrechts D, et al. Role of PlGF in the intra- and intermolecular cross talk between the VEGF receptors Flt1 and Flk1. Nat Med. 2003;9(7):936–43. https://doi.org/10.1038/nm884 PMID: 12796773
34. Mac Gabhann F, Popel AS. Model of competitive binding of vascular endothelial growth factor and placental growth factor to VEGF receptors on endothelial cells. Am J Physiol-Heart Circ Physiol. 2004;286(1):H153–64.
35. Bruns AF, Herbert SP, Odell AF, Jopling HM, Hooper NM, Zachary IC, et al. Ligand-stimulated VEGFR2 signaling is regulated by co-ordinated trafficking and proteolysis. Traffic. 2010;11(1):161–74. https://doi.org/10.1111/j.1600-0854.2009.01001.x PMID: 19883397
36. Bruns AF, Yuldasheva N, Latham AM, Bao L, Pellet-Many C, Frankel P, et al. A heat-shock protein axis regulates VEGFR2 proteolysis, blood vessel development and repair. PLoS ONE. 2012;7(11):e48539.
37. Fearnley GW, Smith GA, Odell AF, Latham AM, Wheatcroft SB, Harrison MA, et al. Vascular endothelial growth factor A-stimulated signaling from endosomes in primary endothelial cells. Methods Enzymol. 2014;535:265–92. https://doi.org/10.1016/B978-0-12-397925-4.00016-X PMID: 24377929
38. Fearnley GW, Smith GA, Abdul-Zani I, Yuldasheva N, Mughal NA, Homer-Vanniasinkam S, et al. VEGF-A isoforms program differential VEGFR2 signal transduction, trafficking and proteolysis. Biol Open. 2016;5(5):571–83. https://doi.org/10.1242/bio.017434 PMID: 27044325

39. Ewan LC, Jopling HM, Jia H, Mittar S, Bagherzadeh A, Howell GJ, et al. Intrinsic tyrosine kinase activity is required for vascular endothelial growth factor receptor 2 ubiquitination, sorting and degradation in endothelial cells. Traffic. 2006;7(9):1270–82. https://doi.org/10.1111/j.1600-0854.2006.00462.x PMID: 17004325
40. Gampel A, Moss L, Jones MC, Brunton V, Norman JC, Mellor H. VEGF regulates the mobilization of VEGFR2/KDR from an intracellular endothelial storage compartment. Blood. 2006;108(8):2624–31. https://doi.org/10.1182/blood-2005-12-007484 PMID: 16638931
41. Sarabipour S, Kinghorn K, Quigley KM, Kovacs-Kasa A, Annex BH, Bautch VL, et al. Trafficking dynamics of VEGFR1, VEGFR2, and NRP1 in human endothelial cells. PLoS Comput Biol. 2024;20(2):e1011798. https://doi.org/10.1371/journal.pcbi.1011798 PMID: 38324585
42. Nakayama M, Nakayama A, van Lessen M, Yamamoto H, Hoffmann S, Drexler HCA, et al. Spatial regulation of VEGF receptor endocytosis in angiogenesis. Nat Cell Biol. 2013;15(3):249–60. https://doi.org/10.1038/ncb2679 PMID: 23354168
43. Mac Gabhann F, Qutub AA, Annex BH, Popel AS. Systems biology of pro-angiogenic therapies targeting the VEGF system. Wiley Interdiscip Rev Syst Biol Med. 2010;2(6):694–707. https://doi.org/10.1002/wsbm.92 PMID: 20890966
44. Wu FTH, Stefanini MO, Mac Gabhann F, Kontos CD, Annex BH, Popel AS. A systems biology perspective on sVEGFR1: its biological function, pathogenic role and therapeutic use. J Cell Mol Med. 2010;14(3):528–52. https://doi.org/10.1111/j.1582-4934.2009.00941.x PMID: 19840194
45. Fuh G, Garcia KC, de Vos AM. The interaction of neuropilin-1 with vascular endothelial growth factor and its receptor flt-1. J Biol Chem. 2000;275(35):26690–5. https://doi.org/10.1074/jbc.M003955200 PMID: 10842181
46. Mac Gabhann F, Yang MT, Popel AS. Monte Carlo simulations of VEGF binding to cell surface receptors in vitro. Biochim Biophys Acta. 2005;1746(2):95–107. https://doi.org/10.1016/j.bbamcr.2005.09.004 PMID: 16257459
47. Kofler N, Corti F, Rivera-Molina F, Deng Y, Toomre D, Simons M. The Rab-effector protein RABEP2 regulates endosomal trafficking to mediate vascular endothelial growth factor receptor-2 (VEGFR2)-dependent signaling. J Biol Chem. 2018;293(13):4805–17. https://doi.org/10.1074/jbc.M117.812172 PMID: 29425100
48. Mac Gabhann F, Popel AS. Dimerization of VEGF receptors and implications for signal transduction: a computational study. Biophys Chem. 2007;128(2–3):125–39. https://doi.org/10.1016/j.bpc.2007.03.010 PMID: 17442480
49. Harris LA, Hogg JS, Tapia J-J, Sekar JAP, Gupta S, Korsunsky I, et al. BioNetGen 2.2: advances in rule-based modeling. Bioinformatics. 2016;32(21):3366–8. https://doi.org/10.1093/bioinformatics/btw469 PMID: 27402907
50. Incio J, Tam J, Rahbari NN, Suboj P, McManus DT, Chin SM, et al. PlGF/VEGFR-1 Signaling Promotes Macrophage Polarization and Accelerated Tumor Progression in Obesity. Clin Cancer Res. 2016;22(12):2993–3004. https://doi.org/10.1158/1078-0432.CCR-15-1839 PMID: 26861455
51. Ganta VC, Choi M, Farber CR, Annex BH. Antiangiogenic VEGF165b Regulates Macrophage Polarization via S100A8/S100A9 in Peripheral Artery Disease. Circulation. 2019;139(2):226–42. https://doi.org/10.1161/CIRCULATIONAHA.118.034165 PMID: 30586702
52. Boucher JM, Clark RP, Chong DC, Citrin KM, Wylie LA, Bautch VL. Dynamic alterations in decoy VEGF receptor-1 stability regulate angiogenesis. Nat Commun. 2017;8:15699. https://doi.org/10.1038/ncomms15699 PMID: 28589930
53. Clegg W, Mac Gabhann F. Site-specific phosphorylation of VEGFR2 is mediated by receptor trafficking: insights from a computational model. PLOS Comput Biol. 2015;11(6):e1004158.
54. Lampugnani MG, Orsenigo F, Gagliani MC, Tacchetti C, Dejana E. Vascular endothelial cadherin controls VEGFR-2 internalization and signaling from intracellular compartments. J Cell Biol. 2006;174(4):593–604. https://doi.org/10.1083/jcb.200602080 PMID: 16893970
55. Lamalice L, Houle F, Huot J. Phosphorylation of Tyr1214 within VEGFR-2 triggers the recruitment of Nck and activation of Fyn leading to SAPK2/p38 activation and endothelial cell migration in response to VEGF. J Biol Chem. 2006;281(45):34009–20. https://doi.org/10.1074/jbc.M603928200 PMID: 16966330
56. Tan WH, Popel AS, Mac Gabhann F. Computational model of VEGFR2 pathway to ERK activation and modulation through receptor trafficking. Cell Signal. 2013;25(12):2496–510. https://doi.org/10.1016/j.cellsig.2013.08.015 PMID: 23993967
57. Goh LK, Sorkin A. Endocytosis of receptor tyrosine kinases. Cold Spring Harb Perspect Biol. 2013;5(5):a017459. https://doi.org/10.1101/cshperspect.a017459 PMID: 23637288
58. Gourlaouen M, Welti JC, Vasudev NS, Reynolds AR. Essential role for endocytosis in the growth factor-stimulated activation of ERK1/2 in endothelial cells. J Biol Chem. 2013;288(11):7467–80.
59. Wu FTH, Stefanini MO, Mac Gabhann F, Kontos CD, Annex BH, Popel AS. VEGF and soluble VEGF receptor-1 (sFlt-1) distributions in peripheral arterial disease: an in silico model. Am J Physiol Heart Circ Physiol. 2010;298(6):H2174-91. https://doi.org/10.1152/ajpheart.00365.2009 PMID: 20382861
60. Bhattacharya R, Kang-Decker N, Hughes DA, Mukherjee P, Shah V, McNiven MA, et al. Regulatory role of dynamin-2 in VEGFR-2/KDR-mediated endothelial signaling. FASEB J. 2005;19(12):1692–4. https://doi.org/10.1096/fj.05-3889fje PMID: 16049137
61. Lee MY, Skoura A, Park EJ, Landskroner-Eiger S, Jozsef L, Luciano AK, et al. Dynamin 2 regulation of integrin endocytosis, but not VEGF signaling, is crucial for developmental angiogenesis. Development. 2014;141(7):1465–72. https://doi.org/10.1242/dev.104539 PMID: 24598168
62. Starbuck C, Lauffenburger DA. Mathematical model for the effects of epidermal growth factor receptor trafficking dynamics on fibroblast proliferation responses. Biotechnol Prog. 1992;8(2):132–43.
63. Wiley HS, Shvartsman SY, Lauffenburger DA. Computational modeling of the EGF-receptor system: a paradigm for systems biology. Trends Cell Biol. 2003;13(1):43–50. https://doi.org/10.1016/s0962-8924(02)00009-0 PMID: 12480339

64. Alfonzo-Méndez MA, Sochacki KA, Strub M-P, Taraska JW. Dual clathrin and integrin signaling systems regulate growth factor receptor activation. Nat Commun. 2022;13(1):905.
65. Gill A, Kinghorn K, Bautch VL, Mac Gabhann F. Mechanistic computational modeling of sFLT1 secretion dynamics. bioRxiv. 2025;:2025.02.12.637983. https://doi.org/10.1101/2025.02.12.637983 PMID: 40027776
66. Simons M. An inside view: VEGF receptor trafficking and signaling. Physiology (Bethesda). 2012;27(4):213–22. https://doi.org/10.1152/physiol.00016.2012 PMID: 22875452
67. Fong GH, Rossant J, Gertsenstein M, Breitman ML. Role of the Flt-1 receptor tyrosine kinase in regulating the assembly of vascular endothelium. Nature. 1995;376(6535):66–70.
68. Fong GH, Zhang L, Bryce DM, Peng J. Increased hemangioblast commitment, not vascular disorganization, is the primary defect in flt-1 knock-out mice. Development. 1999;126(13):3015–25. https://doi.org/10.1242/dev.126.13.3015 PMID: 10357944
69. Kearney JB, Kappas NC, Ellerstrom C, DiPaola FW, Bautch VL. The VEGF receptor flt-1 (VEGFR-1) is a positive modulator of vascular sprout formation and branching morphogenesis. Blood. 2004;103(12):4527–35. https://doi.org/10.1182/blood-2003-07-2315 PMID: 14982871
70. Roberts DM, Kearney JB, Johnson JH, Rosenberg MP, Kumar R, Bautch VL. The vascular endothelial growth factor (VEGF) receptor Flt-1 (VEGFR-1) modulates Flk-1 (VEGFR-2) signaling during blood vessel formation. Am J Pathol. 2004;164(5):1531–5. https://doi.org/10.1016/S0002-9440(10)63711-X PMID: 15111299
71. Ganta VC, Choi M, Kutateladze A, Annex BH. VEGF165b Modulates Endothelial VEGFR1-STAT3 Signaling Pathway and Angiogenesis in Human and Experimental Peripheral Arterial Disease. Circ Res. 2017;120(2):282–95. https://doi.org/10.1161/CIRCRESAHA.116.309516 PMID: 27974423
72. Domigan CK, Warren CM, Antanesian V, Happel K, Ziyad S, Lee S, et al. Autocrine VEGF maintains endothelial survival through regulation of metabolism and autophagy. J Cell Sci. 2015;128(12):2236–48. https://doi.org/10.1242/jcs.163774 PMID: 25956888
73. Lee S, Chen TT, Barber CL, Jordan MC, Murdock J, Desai S, et al. Autocrine VEGF signaling is required for vascular homeostasis. Cell. 2007;130(4):691–703. https://doi.org/10.1016/j.cell.2007.06.054 PMID: 17719546
74. Jaffe EA. Cell biology of endothelial cells. Hum Pathol. 1987;18(3):234–9. https://doi.org/10.1016/s0046-8177(87)80005-9 PMID: 3546072
75. Imoukhuede PI, Popel AS. Quantification and cell-to-cell variation of vascular endothelial growth factor receptors. Exp Cell Res. 2011;317(7):955–65. https://doi.org/10.1016/j.yexcr.2010.12.014 PMID: 21185287
76. Wu FTH, Stefanini MO, Mac Gabhann F, Popel AS. A compartment model of VEGF distribution in humans in the presence of soluble VEGF receptor-1 acting as a ligand trap. PLoS ONE. 2009;4:e5108.
77. Hoffmann DC, Willenborg S, Koch M, Zwolanek D, Müller S, Becker A-KA, et al. Proteolytic processing regulates placental growth factor activities. J Biol Chem. 2013;288(25):17976–89. https://doi.org/10.1074/jbc.M113.451831 PMID: 23645683
78. Vintonenko N, Pelaez-Garavito I, Buteau-Lozano H, Toullec A, Lidereau R, Perret YG, et al. Overexpression of VEGF189 in breast cancer cells induces apoptosis via NRP1 under stress conditions. Cell Adhes Migr. 2011;5:332–43.
79. Clegg LE, Mac Gabhann F. A computational analysis of in vivo VEGFR activation by multiple co-expressed ligands. PLoS Comput Biol. 2017;13(3):e1005445. https://doi.org/10.1371/journal.pcbi.1005445 PMID: 28319199